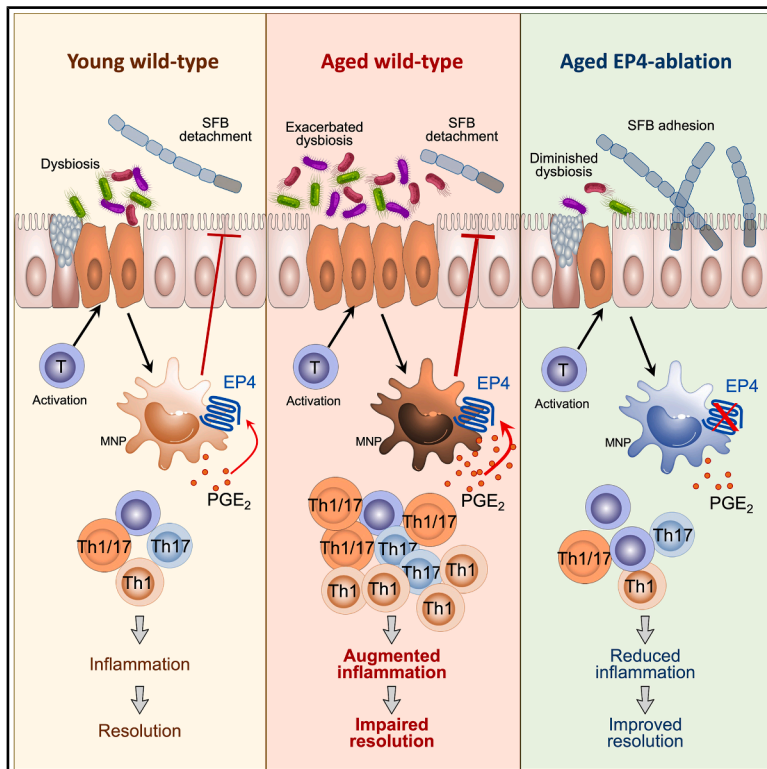


Cell Host & Microbe

Age-related impairment of intestinal inflammation resolution through an eicosanoid-immune-microbiota axis

Graphical abstract



Authors

Marie Goepp, Jemma V. Milburn, Birong Zhang, ..., Mark J. Arends, You Zhou, Chengcan Yao

Correspondence

chengcan.yao@ed.ac.uk

In brief

Goepp et al. demonstrate that endogenous eicosanoid-EP4 signaling mediates age-related impairment of the resolution of intestinal inflammation by disrupting MNP function, hindering SFB adhesion, and increasing pathogenic T cell responses. This study highlights a mechanism by which eicosanoid-altered microbiota affects age-related intestinal inflammation.

Highlights

- Aging shifts eicosanoid metabolism, impairing intestinal inflammation resolution
- MNP-intrinsic EP4 signaling mediates age-related inflammation resolution impairment
- MNP-intrinsic EP4 signaling drives microbiota dysbiosis during intestinal inflammation
- EP4 inhibition retains epithelial adhesion of SFB, aiding inflammation resolution



Article

Age-related impairment of intestinal inflammation resolution through an eicosanoid-immune-microbiota axis

Marie Goepp,^{1,10} Jemma V. Milburn,^{1,10} Birong Zhang,² Yijia Dong,¹ Victoria Tyrrell,² Xiaozhong Zheng,¹ Jennifer M. Marshall,¹ Silvia Bolsega,³ Marijana Basic,³ Laura Glendinning,⁴ Gwo-Tzer Ho,¹ Jack Satsangi,⁵ Richard M. Breyer,⁶ Shuh Narumiya,⁷ Henry J. McSorley,⁸ Jürgen K.J. Schwarze,¹ Christopher J. Anderson,¹ David H. Dockrell,¹ Adriano G. Rossi,¹ André Bleich,³ Christopher D. Lucas,¹ Valerie B. O'Donnell,² Damian Mole,¹ Mark J. Arends,⁹ You Zhou,² and Chengcan Yao^{1,11,*}

¹Centre for Inflammation Research, Institute for Regeneration and Repair, The University of Edinburgh, Edinburgh EH16 4UU, UK

²Systems Immunity University Research Institute and Division of Infection and Immunity, Cardiff University, Cardiff CF14 4XN, UK

³Institute for Laboratory Animal Science, Hannover Medical School, Hannover 30625, Germany

⁴The Roslin Institute & Royal (Dick) School of Veterinary Studies, The University of Edinburgh, Edinburgh EH25 9RG, UK

⁵Translational Gastroenterology Unit, Nuffield Department of Medicine, The University of Oxford, Oxford OX3 9DU, UK

⁶Department of Veterans Affairs, Tennessee Valley Health Authority, and Department of Medicine, Vanderbilt University Medical Center, Nashville, TN 37232, USA

⁷Alliance Laboratory for Advanced Medical Research and Department of Drug Discovery Medicine, Medical Innovation Center, Kyoto University Graduate School of Medicine, Kyoto 606-8507, Japan

⁸Division of Cell Signaling and Immunology, School of Life Sciences, Wellcome Trust Building, The University of Dundee, Dundee DD1 4HN, UK

⁹Edinburgh Pathology, Cancer Research UK Scotland Centre, Institute of Genetics & Cancer, The University of Edinburgh, Institute of Genetics & Cancer, Edinburgh EH4 2XR, UK

¹⁰These authors contributed equally

¹¹Lead contact

*Correspondence: chengcan.yao@ed.ac.uk

<https://doi.org/10.1016/j.chom.2025.04.014>

SUMMARY

Aging manifests a decline of immune function, induces microbiome dysbiosis, drives organ inflammation, and impedes the resolution of inflammation. However, the mechanisms underlying age-related intestinal inflammation remain poorly described. Here, we find that the resolution of T cell-initiated intestinal inflammation is impaired with aging. This impairment is mediated by disrupting the immune-microbiota interplay, controlled by intestinal eicosanoid metabolism. Pharmacologically inhibiting eicosanoid biosynthesis, blocking the prostaglandin E receptor subtype 4 (EP4), or genetically ablating EP4 diminishes age-related impairment of intestinal inflammation resolution. Mechanistically, mononuclear phagocyte-intrinsic eicosanoid-EP4 signaling impedes the resolution of intestinal inflammation through fostering gut microbial dysbiosis and, more importantly, interrupting segmented filamentous bacterial adhesion to the intestinal epithelium. Colonization with EP4-ablated mouse microbiota or segmented filamentous bacteria improves the resolution of intestinal inflammation. These findings reveal that eicosanoid-dependent immune-microbiota interactions impair inflammation resolution in the aged intestine, highlighting potential intervention strategies for improving age-related gut health.

INTRODUCTION

Aging is a significant risk factor for chronic pathologies, organ dysfunction, and loss of regenerative capacity.^{1,2} Inflammatory conditions are commonly worsened by age and associated with microbial dysbiosis, and options for management of these conditions are limited for the elderly.^{3,4} Aging considerably affects the composition and function of intestinal mononuclear phagocytes (MNP)—for instance, recruiting more blood-

derived monocytes to the intestine, which can be differentiated into various MNP subsets and dilutes the population of intestinal resident MNPs.⁵ In addition, aging skews the functionality of intestinal MNPs, leading them to adopt more inflammatory phenotypes.⁶ These changes not only contribute to the development of low-grade inflammation commonly seen in elderly individuals but also modify MNP responses to both internal (e.g., signals from commensal bacteria) and external pathogenic stimuli, including vaccines and therapies. In parallel, the maturation change of



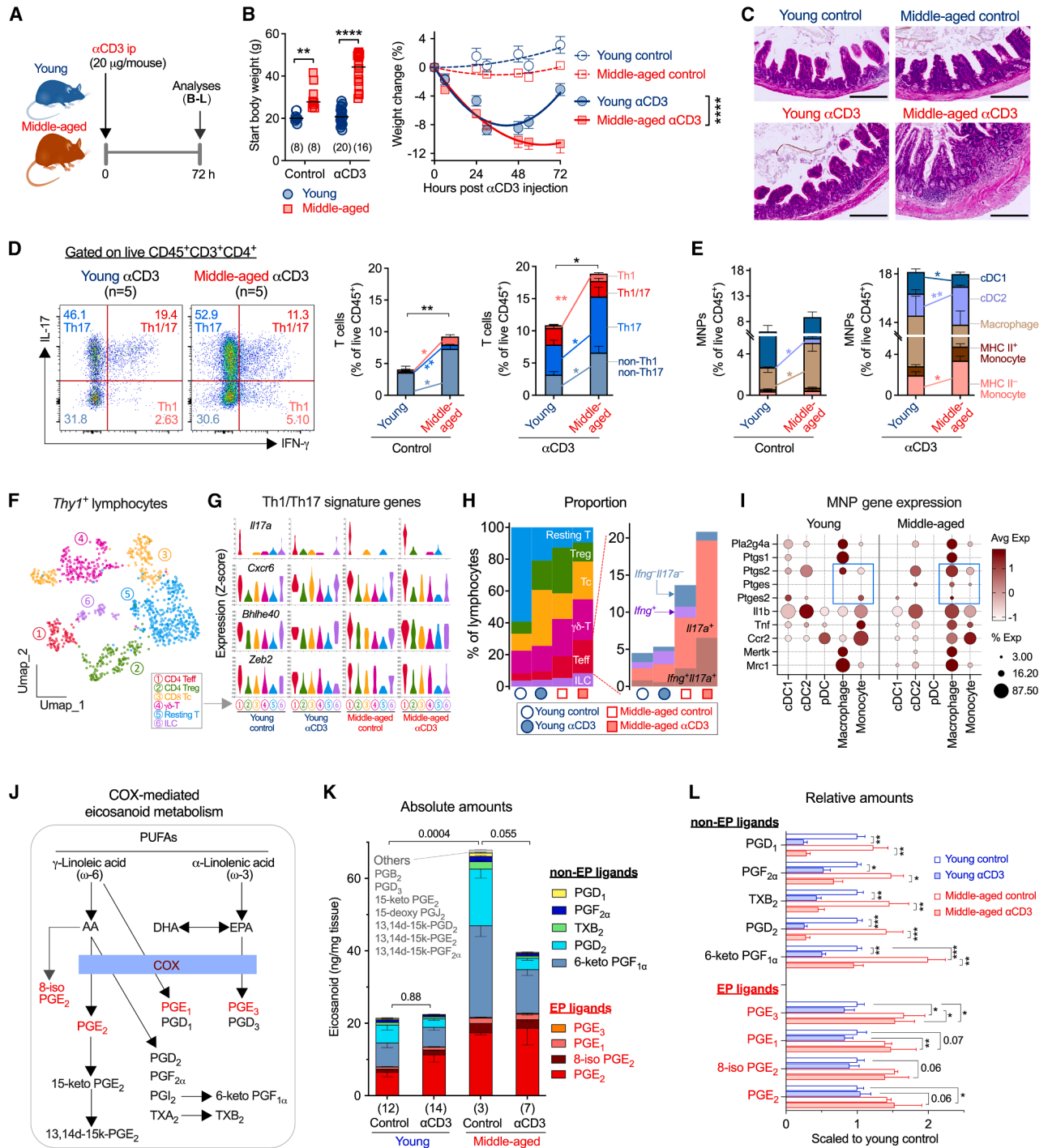


Figure 1. The resolution of T cell-induced intestinal inflammation is impaired with aging, which is associated with an imbalance of eicosanoid metabolism

(A) Experimental setup.
 (B) Baseline body weight and subsequent changes following α CD3 challenge.
 (C) Representative terminal ileal histological images. Scale bar, 200 μ m.
 (D) Representative flow cytometric dot plots and percentages of small intestinal lamina propria (siLP) T cells from α CD3-injected mice.
 (E) Percentages of siLP MNP subsets.
 (F) UMAP analysis of scRNA-seq data for *Thy1*-expressing lymphocyte clusters. Treg, regulatory T cells; Tc, cytotoxic CD8 T cells; ILCs, innate lymphoid cells.
 (G) Expression of Th1 and Th17 signature genes in specific lymphocyte subsets.
 (H) Proportions of each lymphocyte cell subset (left) and *Ilfn*⁻ and/or *Il17a*⁺ expressing T cells (right) among the total lymphocytes by scRNA-seq.

(legend continued on next page)

the immune system creates an environment that favors a shift of the gut microbiota with aging. Age-related microbial dysbiosis, characterized by the expansion of potential pathobionts (such as Enterobacteriaceae and Enterococcaceae) and a reduction in beneficial microorganisms like short-chain fatty acid-producing bacteria, contributes to intestinal dysfunction by increasing epithelial permeability and chronic inflammation, while also exacerbating MNP dysfunction as a result of reciprocal feedback.^{7–9} Crosstalk between MNPs and the microbiota determines mucosal T cell responses and subsequent intestinal inflammation.^{10,11} However, how MNP-microbiota interactions are controlled to influence intestinal inflammation and its resolution in the context of aging remains unknown.

Inflammation is elicited by diverse immunomodulatory factors, including eicosanoids.¹² Eicosanoids are a class of lipid mediators synthesized from 20-carbon polyunsaturated fatty acids (PUFAs). Of which, prostaglandins (PGs), a subgroup of eicosanoids, are oxidized derivatives of arachidonic acid. Their synthesis is catalyzed by cyclooxygenases (COXs), which are encoded by the *PTGS1* and *PTGS2* genes, respectively.¹² Eicosanoids play multifaceted roles in both physiological and pathological processes in health and disease, including influencing aging-related dysfunctions in various organs.^{13–18} Eicosanoids exert their biological functions by binding to their specific receptors. The well-known inflammatory lipid prostaglandin E₂ (PGE₂) binds to its receptors, abbreviated as EP1–4, which are respectively encoded by the *PTGER1–4* genes.¹² We and others have previously described a role of PGE₂ in regulating intestinal epithelial homeostasis through mechanisms involving EP4-expressing epithelial and immune cells.^{19–21} However, it is unclear how aging shapes intestinal eicosanoid metabolism and how immune cell-intrinsic eicosanoid signaling contributes to age-dependent impairment of the resolution of intestinal inflammation. In this study, we sought to examine the role of eicosanoid signaling in age-related intestinal inflammation and the impact of the gut microbiome alteration.

RESULTS

Impairment of the resolution of T cell-induced intestinal inflammation with aging

To study T cell-initiated intestinal inflammation and its resolution, we injected young wild-type (WT) mice intraperitoneally (i.p.) with an agonistic anti-mouse CD3 ϵ monoclonal antibody (α CD3), a widely used animal model^{21–25} that causes small intestinal damage and T cell-dependent inflammation followed by spontaneous recovery (Figure S1). To examine the impacts of aging, we injected young (2–3-month-old) and middle-aged (11–15-month-old) mice with α CD3 (20 μ g per mouse) (Figure 1A). Despite receiving a lower dose of α CD3 per body weight than

young mice, middle-aged mice exhibited more pronounced weight loss and severe histopathological changes in the small intestine, with no recovery observed during the experimental time frame, in contrast to young mice (Figures 1B and 1C). Under non-inflammatory controlled conditions, middle-aged mice exhibited an expansion of small intestinal lamina propria (siLP) helper T (Th) cells, including interferon (IFN)- γ -expressing Th1 cells, interleukin (IL)-17-expressing Th17 cells, and IFN- γ /IL-17-coexpressing Th1/17 cells, with more pronounced effects observed in α CD3-treated mice (Figure 1D). In parallel, infiltration of inflammatory MNPs such as monocytes, especially those that do not express major histocompatibility complex class II (MHC class II), was increased in middle-aged compared with young intestines in response to α CD3 (Figure 1E).

To examine the underlying mechanisms that mediate age-related inflammatory immune responses, we performed single-cell RNA sequencing (scRNA-seq) of siLP CD45⁺Ly6G[–] immune cells sorted from young or middle-aged mice challenged with α CD3 (Figure 1A). The cells were clustered into B and plasma cells, T cells, innate lymphoid cells (ILCs) including natural killer (NK) cells, and MNPs (*Ilgax*, *Ilgam*, *Ly6c2*, *Lyz2*, and *Xcr1*) (Figures S2A and S2B). Among these cells, *Thy1*-expressing lymphocytes that were assigned to different treatment groups were allocated into 6 sub-clusters, including CD4 effector T (Teff) cells (expressing Th1 and Th17 signature genes like *Irfng* and *I17a*), CD4 regulatory T cells (Treg, expressing *Tnfrsf4*, *Foxp3*, and *I110*), CD8 cytotoxic T cells (Tc, expressing *Cd8a*, *Cd8b1*, *Nkg7*, and *Gzmb*), $\gamma\delta$ -T cells (*Trdc*, *Trgv2*, and *Trgv1*), resting/naive T cells (*Sell* and *Cd69*), and ILC/NK cells (*Rorc*, *Tbx21*, *Gata3*, *Ncr1*, and no T cell markers) (Figures 1F, S2C, and S2D). The CD4 Teff subset contained cells expressing Th1 and/or Th17 signature genes (e.g., *I17a*, *Cxcr6*, *Bhlhe40*, and *Zeb2*) in young intestines, and this was increased in middle-aged mice, especially after α CD3 treatment (Figure 1G). The proportion of CD4 Teff, $\gamma\delta$ -T, and ILC/NK cells, all of which express type 1 inflammatory genes *Irfng* and *Tbx21*, were increased in aged intestines in response to α CD3 compared with those in young intestines (Figures 1H and S2D). Consistent with the flow cytometric results, aging markedly elevated pathogenic *Irfng*- and *I17a*-coexpressing Th1/17 cells in the intestine (Figure 1H). By contrast, the proportion of non-pathogenic resting/naive T cells decreased with age in both control and anti-CD3-treated mice. Tregs increased with age in control mice, while they decreased in anti-CD3-treated middle-aged mice compared with young counterparts (Figure 1H).

Shaping of intestinal eicosanoid metabolism in aging

We identified five MNP sub-clusters spanning cDC1 (*Xcr1*), cDC2 (*Irf4*), plasmacytoid DC (pDC) (*Bst2* and *Siglech*),

(I) Expression of genes related to eicosanoid metabolism and MNP functions in various MNP subsets. cDC, conventional dendritic cell; pDC, plasmacytoid DC.

(J) Schematic of simplified cyclooxygenase (COX)-mediated eicosanoid metabolism from polyunsaturated fatty acids (PUFAs). Eicosanoids that can bind to PGE receptors are highlighted in red. AA, arachidonic acid; DHA, docosahexaenoic acid; EPA, eicosapentaenoic acid; PG, prostaglandin; TX, thromboxane.

(K) Absolute concentrations of eicosanoid metabolites in ileal tissues, normalized to dry tissue weight. EP ligands, eicosanoids capable of binding to PGE receptors.

(L) Relative eicosanoid abundance, normalized to the young control group in separate experiments.

(B, D, E, K, and L) All data are presented as mean \pm SEM. Numbers in brackets indicate group sizes. Significance is indicated as * p < 0.05, ** p < 0.01, *** p < 0.001, and **** p < 0.0001.

See also Figures S1, S2, and S3.

macrophages (*Adgre1*, *ApoE*, and *C1qa/b/c*), and monocytes (*Ly6c2* and *S100a4*) (Figures S2E and S2F). Inflammatory genes (e.g., *Il1b*, *Tnf*, and *Ccr2*) were expressed across MNP subsets in young intestines, and their expression in macrophages was up-regulated with aging (Figure 1I). Given that IL-1 β ⁺ macrophage/monocytes initiate pathogenic inflammation through PGE₂ production²⁶ and that *Ptgs1* and *Ptgs2* were exclusively expressed in MNPs compared with other immune cell types (Figure S2B), we examined gene expression related to eicosanoid metabolism in MNP subsets. Polyunsaturated fatty acids, including arachidonic acid, can be metabolized by COXs, lipoxygenases, and epoxygenases.²⁷ The COX pathway-related PG synthase genes (e.g., *Ptgs1*, *Ptgs2*, *Hpgds*, and *Tbxas1*) were highly expressed in most young MNP subsets, with a notable increase in the expression of *Ptgs2*, *Ptges*, and *Ptges2* in middle-aged MNPs, particularly in macrophages (Figures 1I and S2G). These genes, including *Ptgs1* (COX1), *Ptgs2* (COX2), *Ptges* (mPGES), and *Ptges2* (mPGES2), encode key enzymes involved in the biosynthesis of E series PGs, predominantly PGE₂. By contrast, genes associated with lipoxygenase or epoxygenase pathways were barely expressed in both young and middle-aged MNPs (Figure S2G). In corroboration of this, intestinal immune cells, especially MNPs, highly express the PGE receptor EP4 (Figures S2B and S2G). These results suggest that the machinery to drive intestinal eicosanoid metabolism is essentially the COX pathway.

Next, we examined whether an age-related delay of inflammation resolution is linked to changes in eicosanoid metabolism by employing a targeted lipidomic profiling of COX-mediated eicosanoid production in ileal tissues (Figure 1J). Arachidonic acid-derived series 2 of PGs (e.g., PGE₂, PGD₂, and 6-keto PGF_{1 α}) dominated intestinal eicosanoid production, with PGE₂ being most abundant (Figures 1K and S3). Consistent with findings in other organs,¹³ most eicosanoids were elevated in older intestines compared with young controls in the steady state (Figures 1K, 1L, and S3B). Unexpectedly, the levels of PGD₂, PGF_{2 α} , 6-keto PGF_{1 α} , and TXB₂ were reduced by α CD3 in both young and middle-aged mice (Figures 1K, 1L, and S3B). Interestingly, the levels of E series PGs (including PGE₂, PGE₁, and PGE₃) and 8-iso PGE₂, which all can bind to EP receptors, were increased with α CD3 treatment and age (Figures 1K, 1L, and S3B). These results indicate that eicosanoid metabolism is altered with aging and inflammation and that endogenous, EP-binding eicosanoids may mediate age-related impairment of resolution in T cell-initiated intestinal inflammation.

Enhanced COX pathway gene expression is associated with intestinal inflammation in humans

To investigate gene expression related to COX-mediated eicosanoid metabolic pathways (Figure S4A) in human gut inflammation, we analyzed public transcriptomic datasets from intestinal biopsies of Crohn's disease (CD) patients.²⁸ Genes involved in E series PG biosynthesis and transport were overexpressed in CD intestines but downregulated after successful anti-tumor necrosis factor (TNF) therapy, remaining unchanged in refractory patients (Figures 2A and S4B). Conversely, genes for PGE₂ degradation (e.g., *HPGD*) were downregulated in inflamed tissues (Figure S4B). We further analyzed public scRNA-seq datasets of intestinal samples taken from patients with

CD²⁹ or intestinal inflammation induced by immune checkpoint blockade (ICB) therapy.³⁰ Human PGE₂ synthase genes (*PTGS1*, *PTGS2*, and *PTGES*) were predominantly expressed in myeloid cells, and they were elevated in IL1B^{high} inflammatory myeloid cells compared with *MERTK*^{high} residential myeloid cells in ICB-induced colitis (Figures 2B–2D). These data suggest that the inflamed human gut exhibits increased PGE₂ biosynthesis and secretion, leading to elevated PGE₂ levels in the extracellular microenvironment, and that inflammatory myeloid cells are likely to be the main cellular source of endogenous PGE₂ in inflamed intestines.

Moreover, pathogenic Th1/17 cell-related genes (e.g., *IFNG*, *IL1B*, *IL1R1*, *IL23A*, *TBX21*) were positively correlated with PGE₂ signatures, consisting PGE₂ synthases (*PTGS1*, *PTGS2*, *PTGES2*) and receptors (*PTGER2*, *PTGER4*), and negatively correlated with *HPGD* expression in the intestines of CD patients, but showed no such correlations in control intestines without inflammatory bowel disease (IBD) (Figure S4C). We further examined a Nanostring dataset³¹ and found that compared with normal tissues, intestinal biopsies from ICB-induced colitis showed increased expression of inflammatory MNPs and pathogenic Th1/17 signatures, positively correlated with *PTGS2* (Figures 2E and 2F). In contrast, signatures of homeostatic MNPs were reduced and negatively correlated with *PTGS2*. Homeostatic Th17 signature genes (*IL17A*, *MAF*, *IL10*) remained unchanged and showed no significant correlation with *PTGS2* expression (Figures 2E and 2F). Together, these results suggest that COX-dependent eicosanoid metabolism is heightened in inflamed human intestines, which is associated with upregulation of inflammatory MNP and pathogenic T cell genes.

Eicosanoid-EP4 signaling impairs the resolution of T cell-initiated intestinal inflammation

To examine the roles of eicosanoid pathways in intestinal inflammation and its resolution, we employed pharmacological and genetic approaches targeting eicosanoid-EP4 signaling (Figure 3A). Firstly, indomethacin, a non-selective COX inhibitor that inhibits intestinal PG biosynthesis,³² prevented α CD3-induced body weight loss, intestinal Teff cell infiltration, and cytokine production (Figures S5A and S5B). Intestinal Treg cells were also increased by α CD3 as expected, but this was not affected by COX inhibition (Figure S5B). Thus, our results suggest that endogenous eicosanoids promote T cell-initiated intestinal pathology.

Our scRNA-seq results showed that among nine PG receptor genes, EP4 (encoded by *Ptger4*) was highly expressed in intestinal immune cells, especially in MNPs (Figures S2B and S2G). To examine whether eicosanoids mediate intestinal inflammation through EP4 and EP2 (which share downstream signaling with EP4), we injected α CD3 into young mice deficient in EP2 (EP2KO),³³ mice with heterozygous deletion of EP4,³⁴ and WT controls. EP4 heterozygous knockout (KO) is sufficient to inhibit EP4 downstream biological actions *in vivo*.^{20,35} WT and EP2KO mice developed intestinal inflammation, as evidenced by weight loss, histopathological changes, and loss of goblet cells, while such inflammation was not observed in EP4 heterozygous mice (Figures 3B and 3C). Pharmacological EP4 blockade using a highly selective antagonist, L-161,982, similarly diminished α CD3-induced mucosal inflammation and inflammatory T cell

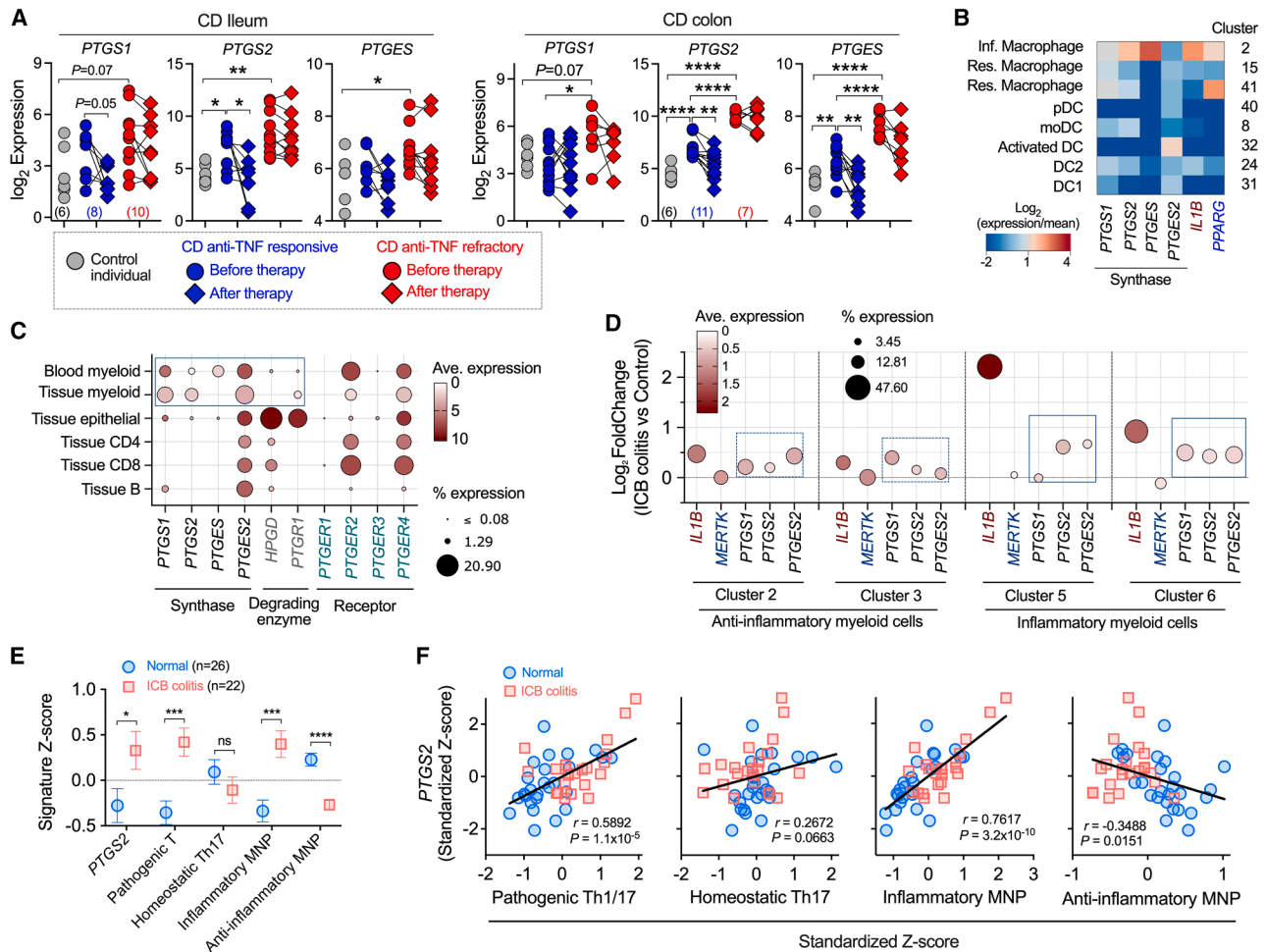


Figure 2. Upregulation of genes related to PGE biosynthesis in human intestinal inflammation

(A) Expression of genes for PGE biosyntheses in ileum and colon biopsies from healthy controls or patients with Crohn's disease (CD) before and after anti-TNF treatment. Raw gene expression data were obtained from the Gene Expression Omnibus (GEO: GSE16879).

(B) Expression of genes for PGE biosyntheses in intestinal MNP subsets from CD patients. Raw data were retrieved from the Gene Expression Omnibus (GEO: GSE134809).²⁹

(C and D) Expression of genes for PGE synthases, degrading enzymes, and receptors (C) and relative gene expression in homeostatic (*MERTK*^{hi}) and inflammatory (*IL1B*^{hi}) myeloid cells (D) of human colon tissues from patients with immune checkpoint blockade (ICB) colitis compared with control colon tissues. Raw data were retrieved from the Gene Expression Omnibus (GEO: GSE206301).³⁰

(E and F) Relative expression (E) and correlations (F) between the *PTGS2* gene and immune cell signatures associated with various immune cell subsets in colonic biopsies from patients with ($n = 22$) or without (normal, $n = 26$) ICB colitis. Immune cell signatures were transformed to normalized Z scores. Original expression data were extracted from a published Nanostring dataset.³¹ Data are presented as mean \pm SEM.

(A and E) Significance is indicated as * $p < 0.05$, ** $p < 0.01$, *** $p < 0.001$, **** $p < 0.0001$, or ns (not significant).

See also Figure S4.

infiltration (Figures 3D–3G). Administration of a highly selective EP4 agonist, L-902,688, alone had little effect on α CD3-induced intestinal inflammation in EP4-WT mice (Figure S5C), likely due to EP4 being already activated by high levels of endogenous ligands (e.g., PGE₂) in the intestine (Figure 1K). Interestingly, administering this EP4 agonist into indomethacin-treated WT mice, where endogenous eicosanoid production was inhibited, not only reversed the protective effects of indomethacin but further exacerbated the condition, leading to a high mortality rate (Figures 3H and 3I). We further examine whether targeting eicosanoid-EP4 signaling improves the resolution of T cell-initiated intestinal inflammation. Anti-CD3 induces acute epithelial

injury within 4–6 h and establishes intestinal inflammation after 24–30 h post injection. Pharmacologically blocking COXs or EP4 at different stages markedly reduced intestinal inflammation (Figures 3J–3M). These results reveal that endogenous eicosanoid-EP4 signaling fosters T cell-initiated intestinal inflammation and delays its resolution.

MNP-intrinsic EP4 impairs the resolution of intestinal inflammation by reprogramming inflammation-resolving MNPs

Since EP4 is expressed in various immune cell types (Figure S1B), we next examined in which specific immune cell

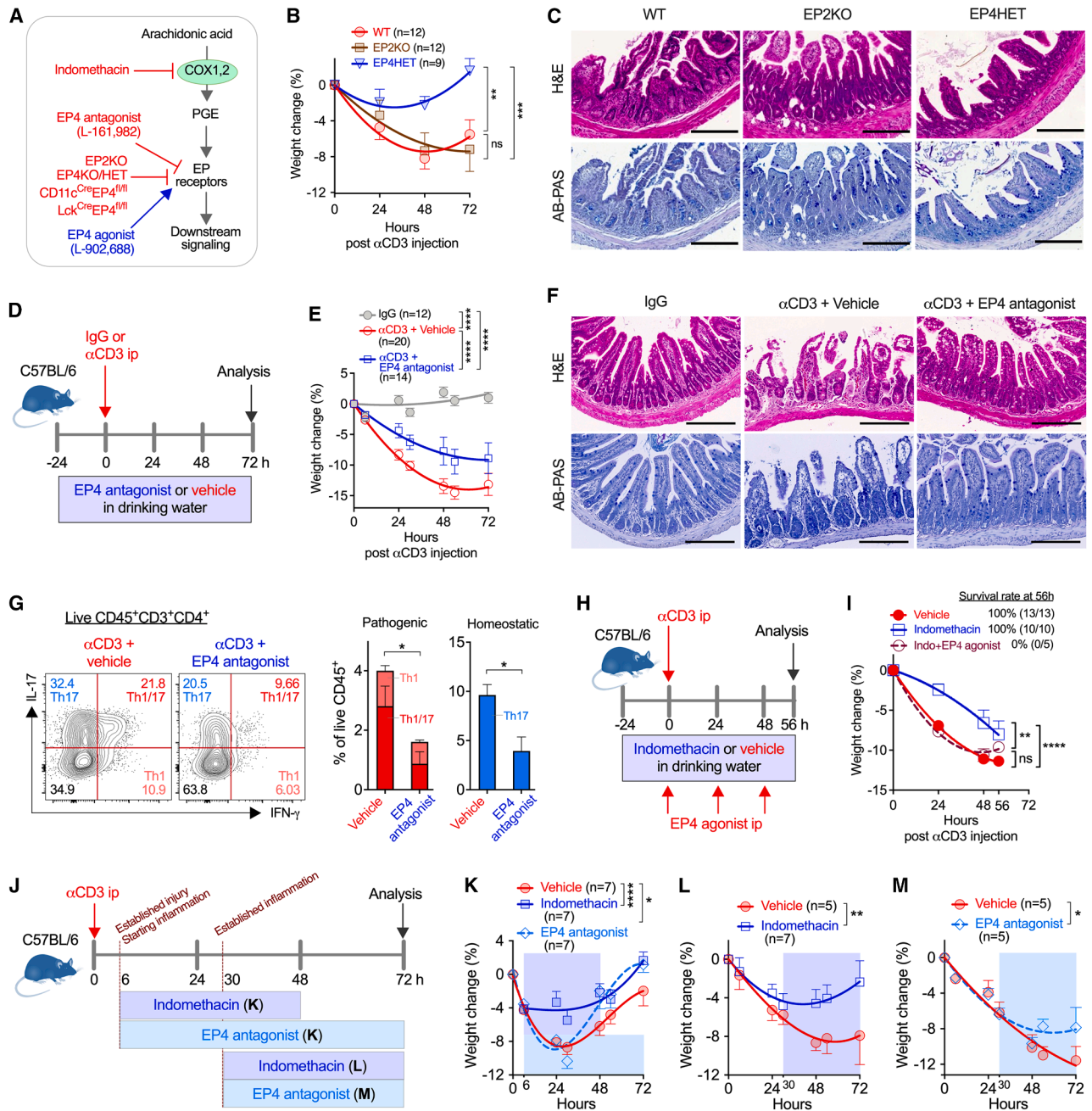


Figure 3. Endogenous eicosanoid-EP4 signaling impairs the resolution of T cell-driven small intestinal inflammation

(A) Schematic of strategies for targeting PGE biosynthesis and receptor signaling.

(B and C) Changes in body weight (B) and representative terminal ileal histological images (C) following α CD3 challenge in young wild-type (WT), EP2 knockout (EP2KO), and EP4 heterozygous knockout (EP4HET) mice. Scale bar, 200 μ m.

(D) Experimental setup.

(E and F) Changes in body weight following α CD3 challenge (E) and representative terminal ileal histological images (F). Scale bar, 200 μ m.

(G) Left: representative flow cytometric dot plots of siLP Th1, Th17, and Th1/17 cells. Right: accumulative percentages of pathogenic (Th1 and Th1/17) and homeostatic (Th17) cells (n = 7 each).

(H and I) Experimental setup (H) and changes in body weight and survival rate at 56 h following α CD3 challenge (I).

(J–M) Experimental setup (J) and changes in body weight following α CD3 challenge (K–M).

(B, E, G, I, and K–M) All data are presented as mean \pm SEM. Numbers in brackets indicate group sizes. Significance is indicated as *p < 0.05, **p < 0.01, ***p < 0.001, ****p < 0.0001, or ns (not significant).

See also Figure S5.

type EP4 signaling was essential for mediating intestinal inflammation. We have previously shown that T cell-intrinsic EP4 signaling promotes pathogenic Teff cell development and T cell-driven inflammation in various tissues.^{36–38} Compared with control EP4^{fl/fl} mice,³⁹ T cell-specific EP4 deficiency (i.e., Lck^{Cre}EP4^{fl/fl})^{36–38} had few effects on α CD3-induced intestinal inflammation or intestinal IFN- γ ⁺ T cells (including IFN- γ ⁺IL-17⁻ Th1 and IFN- γ ⁺IL-17⁺ Th1/17 cells) but significantly reduced IFN- γ ⁻ T cells (including IFN- γ ⁻IL-17⁺ Th17 and IFN- γ ⁻IL-17⁻ non-Th1/Th17 cells) (Figures S6A–S6D). Compared with IFN- γ ⁻ T cells, IFN- γ ⁺ T cells (especially IFN- γ ⁺IL-17⁺ Th1/17 cells) were hyperactivated, as evidenced by increased cell size (larger forward scatter area [FSC-A]), Ki-67 expression, and intracellular cytokine (Figure S6E). This aligns with recent reports indicating that IFN- γ ⁺ T (especially IFN- γ ⁺IL-17⁺ Th1/17) cells are more pathogenic, while IFN- γ ⁻ T (including IFN- γ ⁻IL-17⁺ Th17) cells are generally homeostatic or non-pathogenic in the intestine.^{40,41} These findings indicate that T cell-specific EP4 signaling does not impact pathogenic Teff cells and therefore does not alter T cell-driven intestinal inflammation.

Given that MNP-intrinsic eicosanoid-EP4 signaling inhibits intestinal Treg responses,³² we examined whether EP4 fosters Teff cell responses through MNPs. To this end, we ablated EP4 specifically in MNPs by crossing EP4-floxed mice with CD11c-Cre-EGFP mice⁴² and administered α CD3 into separately housed EP4^{fl/fl} or CD11c^{Cre}EP4^{fl/fl} mice. MNP-specific EP4 deficiency reduced α CD3-induced intestinal inflammation, as evidenced by fewer histopathological changes, less goblet cell loss, and decreased pathogenic IFN- γ ⁺ T cells, while non-pathogenic T cells, including Foxp3⁺ Tregs, remained unchanged (Figures 4A–4C). Thus, MNP-intrinsic eicosanoid-EP4 signaling plays a critical role in mediating pathogenic T cell-induced intestinal inflammation.

To examine the role of MNP-intrinsic EP4 signaling in T cell-mediated intestinal inflammation, we performed bulk RNA-seq analysis of ileal tissues from CD11c^{Cre}EP4^{fl/fl} and EP4^{fl/fl} mice 72 h post α CD3 challenge. Consistent with pathological changes, MNP-specific EP4 deficiency downregulated genes related to neutrophil activation, stress responses, and cell growth (Figures S7A–S7C). Conversely, this deficiency upregulated genes involved in immune tolerance (*Cd83* and *Ccr7*), anti-inflammatory responses (*Siglecg*, *Dio1*, and *S100g*), MHC molecules, intestinal immunoglobulin A (IgA) production (e.g., *Aicda*, *Ms4a1*, *Cd79a*, and *Fcer2a*), goblet cell maturation, entero-protection (*Nt5e* and *Ada*), barrier function (*Spink1* and *Reg3a*), and epithelial repair (*Flt3l*, *Wnt5b*, *Wnt6*, and *Ctnna3*) (Figures S7A–S7F).

Additionally, MNP-specific EP4 deficiency downregulated genes involved in PGE biosynthesis (e.g., *Pla2g2e*) and efflux transport (e.g., *Abcc1* and *Abcc4*), while upregulating *Hpgd* (Figure S7B). Notably, this deficiency enriched pathways related to peroxisome proliferator-activated receptor (PPAR) signaling and fatty acid metabolism, as well as macrophage functions including killing and removal of bacteria and dead cells. These processes encompass phagocytosis, endocytosis, lysosome function, lipid metabolism, and oxidative phosphorylation (Figure 4D). The *Hpgd* gene encodes 15-hydroxyprostaglandin dehydrogenase (15-PGDH) that catalyzes the conversion of PGE₂ to 15-keto-PGE₂, a natural activator of PPAR γ .⁴³ In turn,

PPAR γ reduces PGE₂ levels by inhibiting COX enzymes and upregulating 15-PGDH,⁴⁴ creating a regulatory feedback loop to promote alternative activation of macrophages to adopt anti-inflammatory properties.⁴⁵ The enrichment of PPAR pathway genes in CD11c^{Cre}EP4^{fl/fl} ilea was linked to downregulation of inflammatory MNP signatures alongside upregulation of anti-inflammatory MNP signatures (Figures S7E and S7F). This was corroborated in bone marrow-derived CD11c⁺ MNPs, which demonstrated that PGE₂ and EP4 agonists significantly decreased expression of PPAR γ and homeostatic macrophage markers (e.g., CD206) (Figure 4E), while enhancing the expression of inflammatory MNP markers including CD80 and CD86 (Figure S7G). Intestinal PPAR γ , including in MNPs, reduces mucosal inflammation, at least partially by normalizing gut microbial dysbiosis (such as by limiting *E. coli* expansion).^{46,47} Indeed, activation of PPAR γ with the selective agonist Rosiglitazone significantly reduced T cell-initiated intestinal inflammation and mitigated the effects of MNP-specific EP4 deficiency (Figures 4F and 4G). Together, these results indicate that MNP-intrinsic eicosanoid-EP4 signaling promotes T cell-initiated intestinal inflammation, at least partly by reprogramming MNPs and downregulating the PPAR γ pathway.

MNP-intrinsic eicosanoid-EP4 signaling alters the intestinal microbiota during inflammation

In contrast to separately housed mice, co-housed EP4^{fl/fl} and CD11c^{Cre}EP4^{fl/fl} mice displayed similar pathology following α CD3 challenge (Figure 4H), indicating the involvement of the gut microbiota in EP4-influenced intestinal inflammation. To examine how EP4 impacts the gut microbiota, we performed shotgun metagenomic sequencing of the ileal microbiota from mice 3 days after administration of α CD3 with or without an EP4 antagonist. Compared with IgG controls, the administration of α CD3 tended to reduce gut microbial α -diversity (richness and evenness, as measured by Shannon and Simpson indices) and significantly altered β -diversity (microbial composition, as measured by Bray-Curtis dissimilarity), effects that were nearly reversed by EP4 antagonism (Figure 5A). Similarly, EP4 ablation in MNPs partially reversed α CD3-induced changes in β -diversity but not α -diversity (Figure 5B). Notably, α CD3 treatment reduced the abundance of most anaerobic and aerobic commensal bacteria, including *Clostridia*, while promoting dysbiotic indicators such as *Escherichia*, particularly *E. coli*. These changes were also reversed by blocking EP4 signaling (Figures 5A and 5B). Moreover, α CD3-induced microbiota dysbiosis was mitigated by COX inhibition but reversed by EP4 agonism (Figure 5C). We performed metagenomic sequencing of the ileal microbiota from anti-CD3-treated young and middle-aged mice. In line with the increases in EP4-binding eicosanoids in middle-aged intestines (Figure 1K), microbial α - and β -diversity significantly decreased with age. This change was marked by a reduction in various *Clostridial* species and an increase in dysbiotic indicators, including *E. coli* bloom (Figure 5D). Furthermore, inhibiting EP4 signaling increases the abundance of *Candidatus Arthromitus* (more commonly referred to as segmented filamentous bacteria [SFBs]), whereas enhancing it reduces SFB levels in middle-aged mice (Figures 5A–5D). These data suggest that intestinal eicosanoid-EP4 signaling mediates microbial dysbiosis in T cell-initiated mucosal inflammation.

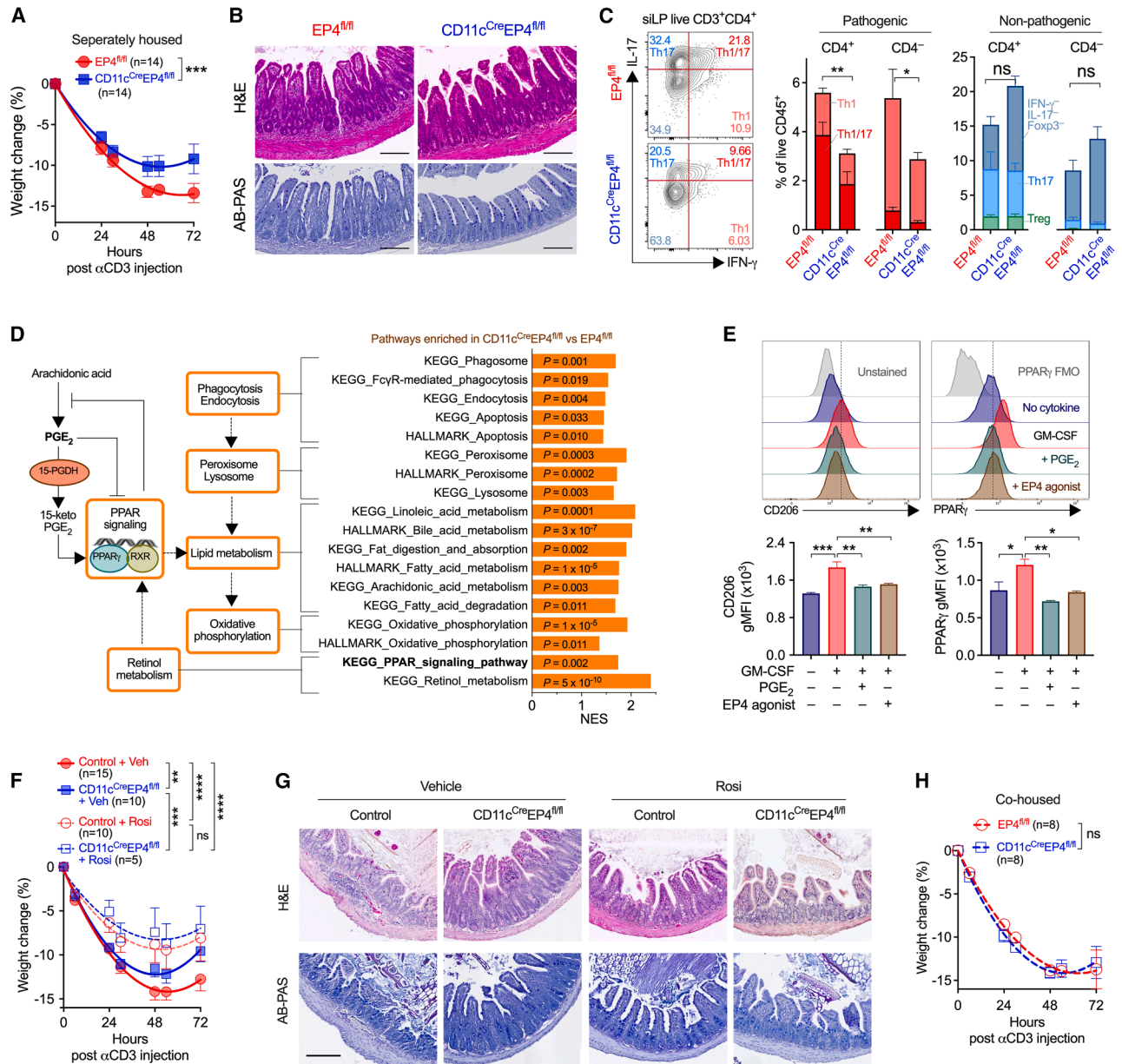


Figure 4. MNP-intrinsic eicosanoid-EP4 signaling impairs the resolution of intestinal inflammation through inhibition of the PPAR γ pathway

(A) Changes in body weight of separately housed EP4^{fl/fl} and CD11c^{Cre}EP4^{fl/fl} mice following α CD3 challenge.

(B) Representative terminal ileal histological images. Scale bar, 200 μ m.

(C) Representative flow cytometric dot plots and percentages of pathogenic and non-pathogenic T cells. EP4^{fl/fl} (n = 5), CD11c^{Cre}EP4^{fl/fl} (n = 9).

(D) Visualization of PPAR signaling-mediated interactions between PGE₂ metabolism and cellular metabolic dynamic pathways (left), and gene enrichment assays of lipid metabolism-associated pathways specifically enriched in CD11c^{Cre}EP4^{fl/fl} (n = 4) compared with EP4^{fl/fl} (n = 6) ilea by bulk RNA-seq (right).

(E) Expression histogram and geometric mean fluorescence intensity (gMFI) of CD206 and PPAR γ in bone marrow-derived MNPs stimulated with indicated conditions for 24 h. FMO, fluorescence minus one.

(F and G) Changes in body weight in mice treated as indicated following α CD3 challenge (F) and representative terminal ileal histological images (G). Rosi, rosiglitazone. Scale bar, 200 μ m.

(H) Changes in body weight of co-housed EP4^{fl/fl} and CD11c^{Cre}EP4^{fl/fl} mice following α CD3 challenge.

(A, C, E, F, and H) All data are presented as mean \pm SEM. Numbers in brackets indicate group sizes. Significance is indicated as *p < 0.05, **p < 0.01, ***p < 0.001, ****p < 0.0001, or ns (not significant).

See also [Figures S6](#) and [S7](#).

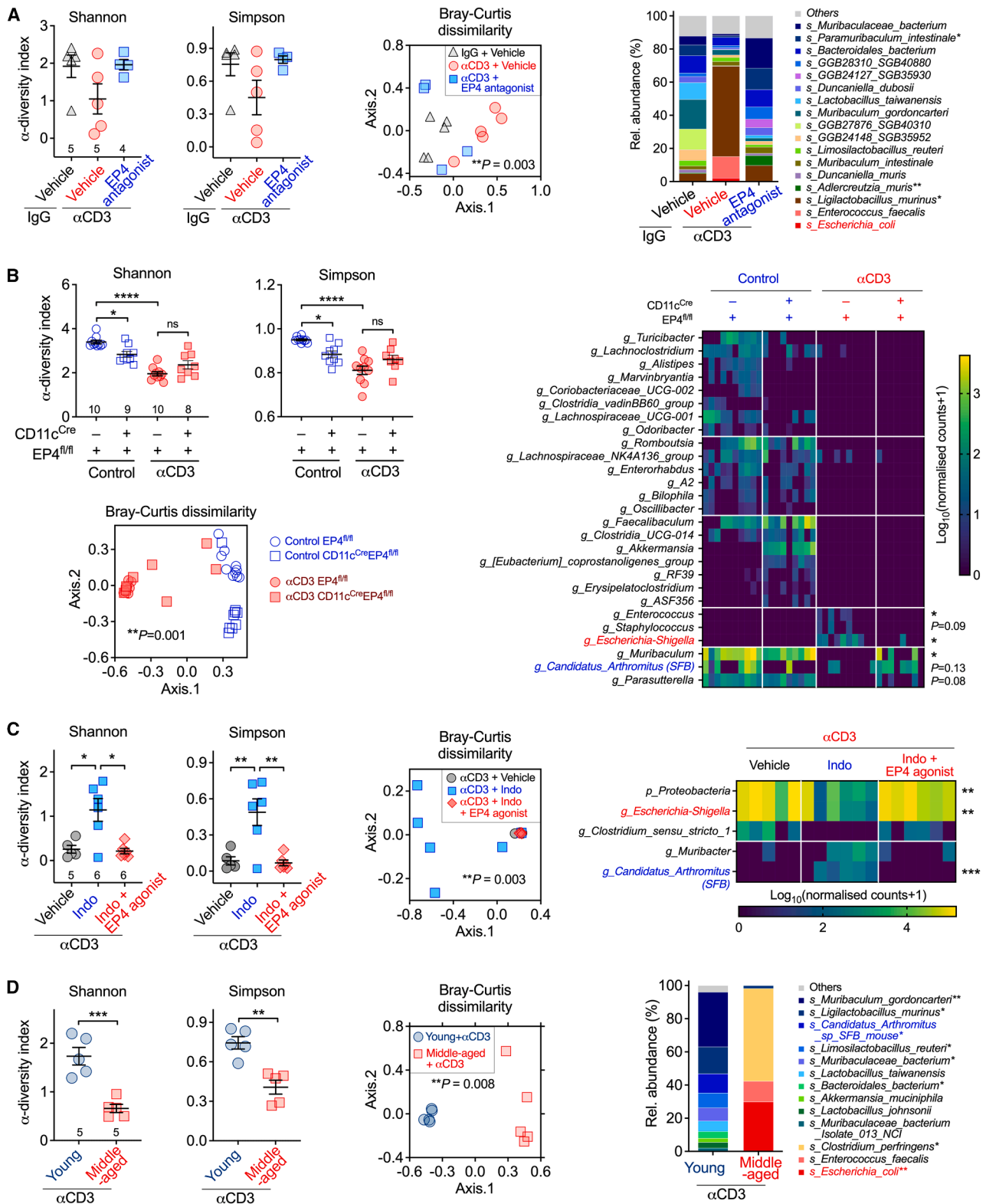


Figure 5. MNP-intrinsic eicosanoid-EP4 signaling alters the intestinal microbiota during T cell-initiated inflammation

(A) Alpha- and beta-diversity indices and relative abundances of bacterial species in the ileal microbiota from young mice treated as illustrated in Figure 3D by shotgun metagenomic sequencing. Statistics in the stacked bar graph show comparisons between the α CD3 + vehicle group and the α CD3 + EP4 antagonist group.

(legend continued on next page)

MNP-intrinsic EP4 signaling mediates age-related impairment of intestinal inflammation resolution

To investigate whether endogenous eicosanoid-EP4 signaling mediates age-related impairment of inflammation resolution and associated microbial dysbiosis, we administered α CD3 into young and middle-aged WT, EP2KO, or EP4KO mice. Consistent with our findings in Figure 1, middle-aged WT mice exhibited more severe responses to α CD3 and impaired resolution of intestinal inflammation, as evidenced by unresolved body weight loss, exacerbated histopathological changes, and more goblet cell loss compared with young WT mice (Figures 6A and 6B). The response to α CD3 in middle-aged EP2KO mice was almost identical to that of middle-aged WT mice (Figures 6A and 6B), further suggesting that EP2 is not essential. Notably, middle-aged EP4KO mice responded similarly to young EP4KO mice, showing resistance to the α CD3 challenge with reduced body weight loss, less intestinal inflammation, and diminished goblet cell loss (Figures 6A and 6B). Furthermore, pharmacologically blocking EP4 significantly attenuated α CD3-induced intestinal inflammation in middle-aged WT mice (Figures 6C and 6D), indicating a critical role of endogenous eicosanoid-EP4 signaling in the age-related impairment of intestinal inflammation resolution.

Consistent with our previous findings, the resolution of CD3-induced intestinal inflammation was impaired in middle-aged EP4^{fl/fl} mice compared with young EP4^{fl/fl} mice. This age-related impairment in resolution was reversed by MNP-specific EP4 deficiency, which was associated with decreased numbers of intestinal inflammatory T cells and monocytes (Figures 6E–6H). Additionally, the age-related reduction of SFB and expansion of *E. coli* in the EP4^{fl/fl} ilea were also reversed in the middle-aged CD11c^{Cre}EP4^{fl/fl} intestines (Figure 6I). The abundances of ileal SFB and *E. coli* were negatively and positively correlated with the severity of intestinal inflammation (e.g., body weight loss) respectively (Figure 6J). These results demonstrate that MNP-intrinsic eicosanoid-EP4 signaling mediates the age-related impairment of intestinal inflammation resolution.

EP4 ablation retains SFB adhesion to the intestinal epithelium, facilitating the resolution of intestinal inflammation

To further investigate the relationships between EP4-mediated microbiota and T cell-initiated intestinal inflammation, we tested the hypothesis that EP4-deficiency-associated microbes may actively contribute to restricting mucosal inflammation. To this end, we collected ileocecal microbiota from CD11c^{Cre}EP4^{fl/fl} or EP4^{fl/fl} mice and transferred them into WT C57BL/6 mice that had been pre-treated with a broad-spectrum antibiotic cocktail (Figure 7A). Compared with mice that received gut microbiota

from EP4^{fl/fl} mice, those that received microbiota from CD11c^{Cre}EP4^{fl/fl} mice exhibited improved resolution of intestinal inflammation following α CD3 challenge, which was associated with a reduction in mucosal pathogenic T cells (Figures 7B–7D).

In the microbial sequencing analyses, we observed an inverse relationship between EP4 signaling and SFB abundance (Figures 5A–5D). SFBs are gram-positive, spore-forming bacteria and are genetically related to the genus *Clostridium*. SFBs intimately attach to the ileal epithelium⁴⁸ and drive the differentiation of homeostatic intestinal Th17 cells.^{49–53} Scanning electron microscopic (SEM) analyses confirmed that, compared with controls, administration of α CD3 completely depleted the ileal epithelial attachment of SFB, an effect that was mitigated by EP4 antagonism or deficiency (Figure 7E). Furthermore, activation of PPAR γ strikingly protected against α CD3-induced SFB detachment from the ileal epithelium (Figure 7E).

SFBs protect against various infections and are related to intestinal pathology through mechanisms including alteration of epithelial cell function, induction of homeostatic intestinal Th17 cells, and suppression of the growth of *Enterobacteriaceae* species, e.g., *E. coli* and *Salmonella*.^{49,54,55} We hypothesized that SFBs promote the resolution of T cell-induced intestinal inflammation. Indeed, vancomycin, which targets gram-positive bacteria including SFBs, increased *E. coli* populations and hindered the resolution of α CD3-induced intestinal inflammation (Figures 7F–7H). Moreover, MNP-specific EP4 deficiency did not improve the resolution of α CD3-induced intestinal inflammation in mice vancomycin-treated mice (Figures 7I and 7J), unlike its beneficial role in mice not treated with vancomycin (Figure 3A). These results suggest that vancomycin-sensitive microbes, possibly including SFBs, play a crucial role in promoting inflammation resolution and that EP4 signaling interacts with microbial factors to modulate this process.

To directly examine the protective effects of SFBs, we transferred gut contents obtained from germ-free (GF) or SFB-monocolonized mice⁵⁶ into vancomycin-pretreated C57BL/6 mice, followed by α CD3 injection (Figure 7K). SFB transfer enhanced the resolution of α CD3-induced intestinal inflammation, as demonstrated by reduced body weight loss, diminished histopathological changes in the ileum, increased goblet cell numbers, and decreased levels of dysbiotic *E. coli* compared with mice that received GF gut contents (Figures 7L–7N). Furthermore, SFB transfer diminished intestinal pathogenic IFN- γ ⁺ T (Th1 and Th1/17) cells in host mice, while, as expected, it increased homeostatic IL-17⁺IFN- γ ⁻ Th17 cells (Figure 7O). Compared with GF content-transferred mice, SFB-transferred mice exhibited fewer inflammatory monocytes and increased macrophages in the intestine (Figure 7P). Together, these results indicate that SFBs actively reduce pathogenic T cell responses and that the detachment of SFBs from the intestinal epithelium

(B) Alpha- and beta-diversity indices and normalized counts of bacteria at the genus level in the ileal microbiota from control or α CD3-treated young EP4^{fl/fl} and CD11c^{Cre}EP4^{fl/fl} mice by 16S rRNA-seq. Statistics in the heatmap show comparisons between α CD3-treated EP4^{fl/fl} and CD11c^{Cre}EP4^{fl/fl} groups.

(C) Alpha- and beta-diversity indices and normalized counts of bacteria at the genus level in the ileal microbiota from young mice treated as illustrated in Figure 3H by 16S rRNA-seq. Statistics in the heatmap show comparisons between the Indo + EP4 agonist group and the Indo group.

(D) Alpha- and beta-diversity indices and relative abundances of bacterial species in the ileal microbiota from young and middle-aged C57BL/6 mice 72 h after administration of α CD3 by shotgun metagenomic sequencing.

(A–D) Numbers in brackets indicate group sizes. Each dot represents one mouse. Significance is indicated as * $p < 0.05$, ** $p < 0.01$, *** $p < 0.001$, **** $p < 0.0001$, or ns (not significant).

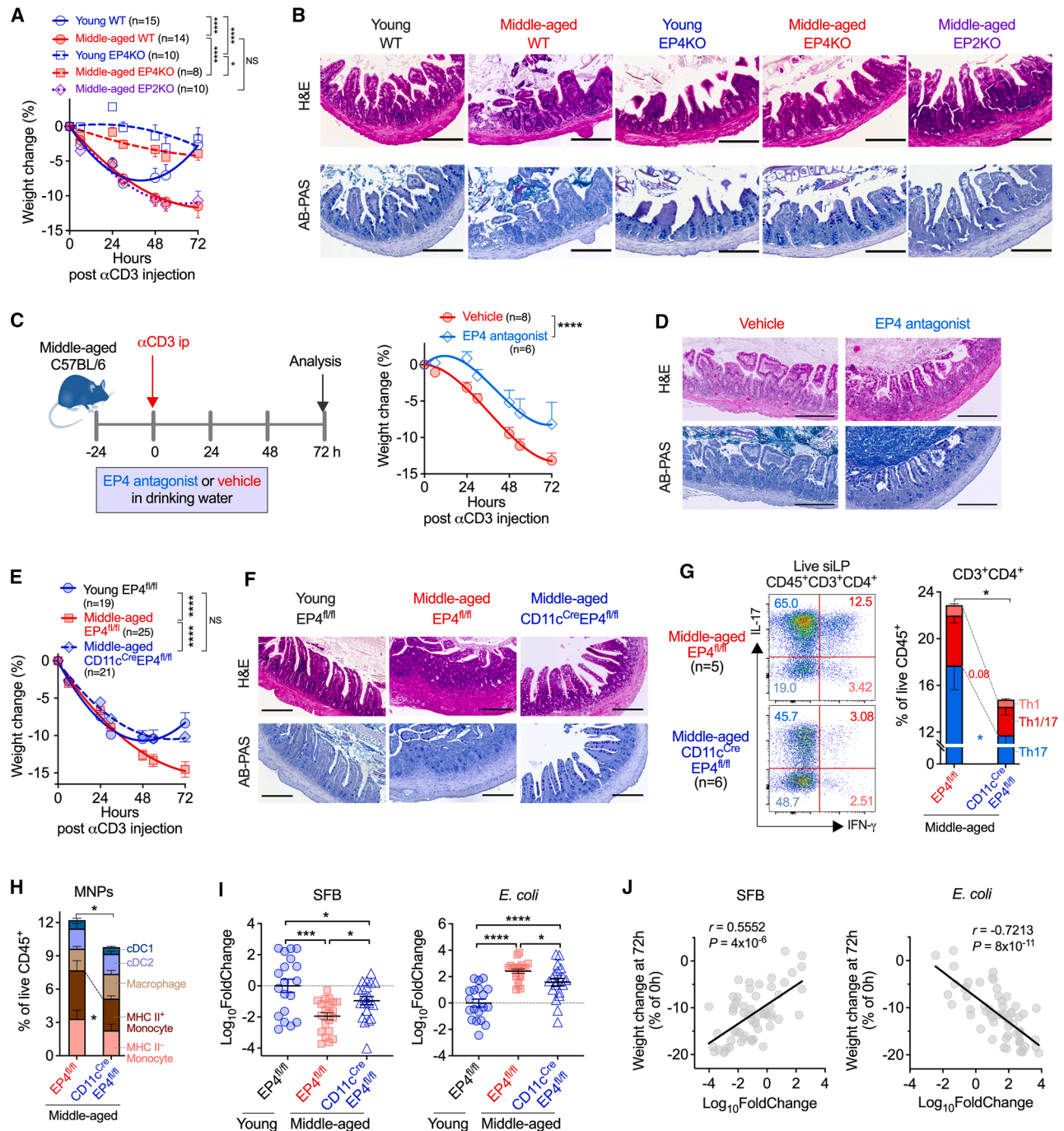


Figure 6. Age-related impairment of intestinal inflammation resolution is mediated by MNP-intrinsic EP4 signaling and associated with alterations in the microbiota

(A and B) Changes in body weight (A) and representative terminal ileal histological images (B) of young and middle-aged WT, EP4KO, and EP2KO mice following α CD3 challenge. Scale bar, 200 μ m.

(C) Experimental setup and changes in body weight following α CD3 challenge.

(D) Representative terminal ileal histological images. Scale bar, 200 μ m.

(E) Changes in body weight of young and middle-aged EP4^{fl/fl} and CD11c^{Cre}EP4^{fl/fl} mice following α CD3 challenge.

(F) Representative terminal ileal histological images. Scale bar, 200 μ m.

(G and H) Percentages of siLP T cell and MNP subsets in α CD3-treated middle-aged EP4^{fl/fl} and CD11c^{Cre}EP4^{fl/fl} mice.

(legend continued on next page)

underlies the impairment of inflammation resolution mediated by eicosanoid-EP4 signaling.

DISCUSSION

Collectively, we reveal a previously unrecognized role of MNP-intrinsic eicosanoid signaling in the age-related impairment of intestinal inflammation resolution. Our findings demonstrate that aging shifts intestinal eicosanoid metabolism to enhance EP4 signaling, which restricts the reparative MNP phenotype. This shift is associated with intestinal microbial dysbiosis, particularly disrupting SFB adhesion to the ileal epithelium. Consequently, this leads to the amplification of mucosal pathogenic T cell responses and impairs the resolution of intestinal inflammation (Figure S8).

Aging has a significant impact on gut inflammatory conditions, including elderly onset CD^{3,4} and adverse gastrointestinal effects of immunotherapy.⁵⁷ It also influences the resolution of inflammation.⁵⁸ Clinically, control of intestinal inflammation results in disease remission and symptom improvement in IBD patients, such as decreased pain and diarrhea, less body weight loss, and enhanced overall health. Our findings indicate that aging is associated with the exacerbation of T cell-initiated intestinal inflammation and the delay in its resolution, which is due to disruption in the balance between pathogenic and homeostatic T cells following anti-CD3 challenge. These results align with observations that older populations frequently experience gastrointestinal problems,^{59,60} particularly following immunotherapy.⁵⁷ Additionally, we found that gene expression related to the biosynthesis of EP4-activating eicosanoids is linked to intestinal inflammation and response to anti-TNF therapy in human CD. Therefore, targeting eicosanoid-EP4 signaling in immune cells, particularly in MNPs, may help alleviate human intestinal inflammation triggered by T cell hyperactivation, such as in CD or induced by immunotherapies or vaccines, although it should be noted that EP4 signaling in other cell types, including epithelial cells and ILCs, can have a protective role in conditions like ulcerative colitis.^{19–21}

More importantly, we demonstrated that the age-related influences on intestinal inflammation are linked to imbalanced eicosanoid metabolism, mediated by signaling through EP4 expressed on MNPs. There is a possibility that this may stem from increased body mass and fat, which is also associated with age. Indeed, high-fat diet administration, which raises body fat, increases intestinal PGE₂⁶¹ and decreases SFB abundance, correlating with an increase in pathogenic IFN- γ ⁺ Th1 cells in the gut.⁵² Furthermore, high-fat diet exposure expands the commensal Enterobacteriaceae, exacerbating pro-IBD-like mucosal inflammation.⁶² These findings indicate a strong correlation between high-fat-diet-mediated increase in body mass (or fat) and the intestinal inflammatory status. However, our retrospective analysis revealed no correlation between initial body mass and the severity of intestinal inflammation in either young or middle-aged EP4 WT mice raised on normal diets (data not

shown). Therefore, further investigation is needed to clarify the relationship between body mass or fat and age-related intestinal inflammation.

Another feature of aging is its impact on the intestinal microbiota.^{7,63,64} Specifically, aging is associated with an increased abundance of potential pathobionts, such as Enterobacteriaceae and *Enterococcus*, along with a decrease in beneficial bacteria in the human intestinal microbiome.⁶⁵ This shift is particularly pronounced in unhealthy aging and age-related disease like IBD.^{66,67} In addition to inducing microbiota dysbiosis characterized by *E. coli* bloom, we found a relationship between MNP-intrinsic eicosanoid-EP4 signaling, SFB depletion, and age-related impairment of the resolution of intestinal inflammation. SFBs have been shown to increase resistance to colonization by potential pathobionts such as Enterobacteriaceae and *Faecalibaculum rodentium*.^{49,68} Furthermore, SFBs promote the development of intestinal Th17 cells.⁴⁹ These SFB-induced Th17 cells are non-pathogenic and possess homeostatic properties, such as producing IL-10, in the intestine.^{51,53} Our findings show that transferring SFB not only increased intestinal homeostatic Th17 cells but also reduced pathogenic IFN- γ -producing T (i.e., Th1 and Th1/17) cells. Although the exact mechanisms by which SFBs promote homeostatic Th17 cells and suppress pathogenic T cells require further investigation, macrophages are suggested to play a role.⁵³

Overall, our research demonstrates that eicosanoid-mediated immune-microbiota interactions exacerbate intestinal inflammation and hinder its resolution, particularly in aging populations. Targeting eicosanoid-EP4 signaling, alongside the disruption of SFB adhesion to the epithelium, offers promising strategies for managing age-related inflammation such as IBD, and immunotherapy-related adverse effects in the intestine.

Limitations of the study

Several limitations exist in this study and warrant further research. First, while this research includes analysis of PGE₂-related gene expression in human intestinal biopsies, the broader implications of PGE₂ signaling on immune-microbiome interactions in human intestinal conditions were not fully examined. Second, the study omitted the influence of body fat in our experimental models. Considering the link between aging, higher eicosanoid production, and body fat, and the impact of increased body fat on intestinal PGE₂ and gut microbiota changes, including reduced SFB,^{52,61} addressing this factor is crucial for advancing our understanding. Finally, the specific and active mechanisms by which PGE₂-EP4 signaling inhibits SFB adhesion during T cell-driven intestinal inflammation remain unclear.

RESOURCE AVAILABILITY

Lead contact

Further information and requests for resources and reagents should be directed to and will be fulfilled by the lead contact, Chengcan Yao (chengcan.yao@ed.ac.uk).

(I) Relative abundances of SFB and *E. coli* in ileal contents by qPCR. Data are normalized and presented as relative log₁₀foldchange to the young EP4^{fl/fl} group.

(J) Correlations of body weight loss and relative abundances of *E. coli* and SFB.

(A, C, E, and G–J) All data are presented as mean \pm SEM. Numbers in brackets indicate group sizes. Significance is indicated as * $p < 0.05$, ** $p < 0.01$, *** $p < 0.001$, **** $p < 0.0001$, or ns (not significant).

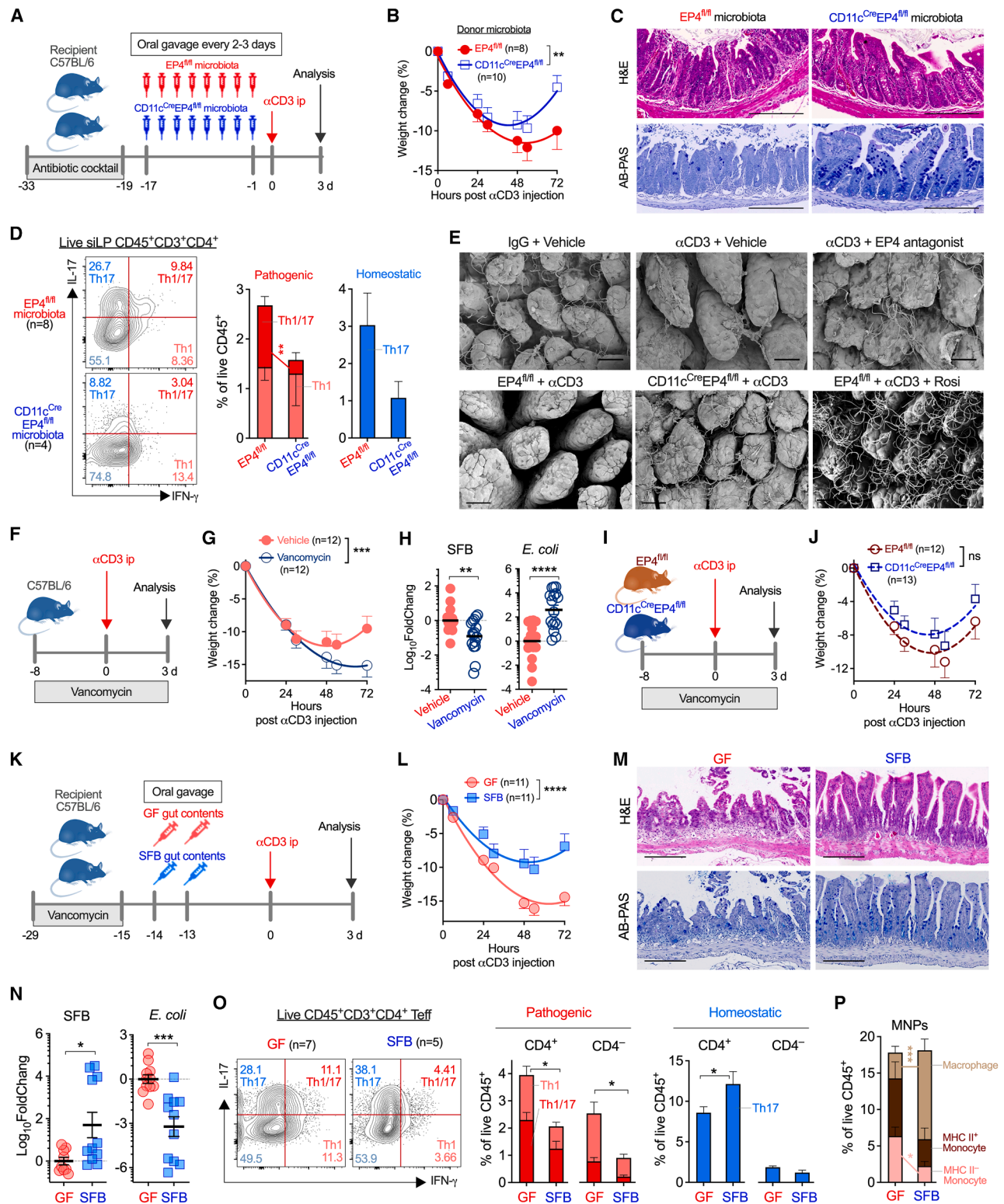


Figure 7. MNP-intrinsic EP4 ablation retains SFB adhesion to the ileal epithelium, facilitating the resolution of intestinal inflammation

(A and B) Experimental setup (A) and changes in body weight following $\alpha CD3$ injection (B).

(C) Representative recipient terminal ileal histological images. Scale bar, 200 μm .

(D) Representative flow cytometric dot plots and accumulative percentages of siLP T cell subsets.

(legend continued on next page)

Materials availability

No new, unique reagents were generated in this study.

Data and code availability

- scRNA-seq data have been deposited in the NCBI Sequencing Read Archive (SRA) under the BioProject PRJNA1109827 (SRA accessions SRX24520233 and SRX24520234). Bulk RNA-seq data have been deposited in the SRA under the BioProject PRJNA978526 (SRA accessions SRS19271684-SRS19271693). 16S rRNA-seq data have been deposited in the SRA under the BioProject PRJNA972542 (SRA accessions SRS19269700-SRS19269753). Shotgun metagenomics sequencing data have been deposited in the European Nucleotide Archive under the PRJEB83270 (SRA accessions ERX13451376-ERX13451388, ERX13451390-ERX13451392, ERX13451394, ERX13451398, ERX13451399, ERX13451401-ERX13451404, ERX13451407, ERX13452515, ERX13453230).
- This paper does not generate original code.
- All additional information required to reanalyze the data reported in this paper is available from the [lead contact](#) upon request.

ACKNOWLEDGMENTS

We thank R. Maizels for helpful support; J. Cash for donating animals; N.B. Cuhe and A. Adams for their assistance with data analysis; the staff at the UOE IRR Flow Cytometry, Single-cell platform, and Histology facilities for assistance with cell sorting, analysis, and histological processes; the staff at the UOE Little France and SCRIM animal facilities for assistance with animal care and husbandry; the staff at the Edinburgh Clinical Research Facility, the Integrated Microbiome Resource (IMR), and Novogene for sequencing services; S. Mitchell (School of Biological Sciences, UOE) and F. Laidlaw (UOE Cryo FIB-SEM facility) for assistance with scanning electron microscopy; and A. Smoczek (Hannover Medical School) for excellent technical assistance with gnotobiotics. We acknowledge the support of the Supercomputing Wales project, which is partly funded by the European Regional Development Fund (ERDF) via the Welsh Government. This work has made use of the computer cluster EDDIE, a resource provided by the Edinburgh Compute and Data Facility (ECDF). A.G.R. was supported by Medical Research Council (MRC) UK grant MR/K013386/1. D.M. was supported by MRC UK grant MR/P008887/1. M.J.A. was supported by the Pathological Society of Great Britain and Ireland grant. S.N. was supported by a collaborative grant to Kyoto University from Ono Pharmaceuticals. R.M.B. was supported by National Institutes of Health grant HL134895. M.B. was supported by German Research Foundation (DFG) project grant 395357507 – SFB 1371. C.Y. was supported by UKRI MRC grant MR/R008167/1 and Cancer Research UK grant C63480/A25246. This article is subject to UKRI's Open Access to Publications policy. Pursuant to those licenses, the author-accepted manuscript of this article can be made freely available under a CC BY 4.0 license immediately upon publication.

AUTHOR CONTRIBUTIONS

C.Y. conceived the study. M.G. and J.V.M. performed the experiments with help from Y.D., V.T., X.Z., and J.M.M. M.G., J.V.M., B.Z., L.G., Y.Z., V.T., C. D.L., and C.Y. analyzed the data. S.B., M.B., G.-T.H., J.S., R.M.B., S.N., H. J.M., J.K.J.S., D.H.D., A.G.R., A.B., V.B.O., D.M., and M.J.A. provided the technical expertise and essential reagents and advised on the experimental

design and data analysis. J.V.M. and C.Y. wrote the manuscript with input from S.N., J.K.J.S., C.J.A., D.H.D., V.B.O., M.J.A., and Y.Z.

DECLARATION OF INTERESTS

The authors declare no competing interests.

STAR★METHODS

Detailed methods are provided in the online version of this paper and include the following:

- [KEY RESOURCES TABLE](#)
- [EXPERIMENTAL MODEL AND STUDY PARTICIPANT DETAILS](#)
 - Animal Experiments
 - Bone marrow-derived MNP culture
- [METHOD DETAILS](#)
 - Intestinal histology
 - Isolation of intestinal lamina propria cells
 - Surface and intracellular staining
 - Oxylin analysis
 - Bulk RNA-seq
 - Single-cell RNA-seq and data analysis
 - 16S rRNA and shotgun metagenomic sequencing
 - Gene expression analysis of human intestinal biopsies
 - Gene expression and real-time qPCR
 - Scanning electron microscopy
- [QUANTIFICATION AND STATISTICAL ANALYSIS](#)

SUPPLEMENTAL INFORMATION

Supplemental information can be found online at <https://doi.org/10.1016/j.chom.2025.04.014>.

Received: July 9, 2024

Revised: February 27, 2025

Accepted: April 15, 2025

Published: May 14, 2025

REFERENCES

1. López-Otín, C., Blasco, M.A., Partridge, L., Serrano, M., and Kroemer, G. (2023). Hallmarks of aging: An expanding universe. *Cell* 186, 243–278. <https://doi.org/10.1016/j.cell.2022.11.001>.
2. Furman, D., Campisi, J., Verdin, E., Carrera-Bastos, P., Targ, S., Franceschi, C., Ferrucci, L., Gilroy, D.W., Fasano, A., Miller, G.W., et al. (2019). Chronic inflammation in the etiology of disease across the life span. *Nat. Med.* 25, 1822–1832. <https://doi.org/10.1038/s41591-019-0675-0>.
3. Everhov, Å.H., Halfvarson, J., Myrelid, P., Sachs, M.C., Nordenvall, C., Söderling, J., Ekbohm, A., Neovius, M., Ludvigsson, J.F., Askling, J., et al. (2018). Incidence and Treatment of Patients Diagnosed With Inflammatory Bowel Diseases at 60 Years or Older in Sweden. *Gastroenterology* 154, 518–528.e15. <https://doi.org/10.1053/j.gastro.2017.10.034>.

(E) Scanning electron microscopic (SEM) images of SFB adhesion to the ileal epithelium in various mice treated as indicated. Scale bar, 50 μ m.

(F–H) Experimental setup (F), changes in body weight (G), and relative abundances of SFB and *E. coli* in the ileal contents (H) of young C57BL/6 mice treated as indicated.

(I and J) Experimental setup (I) and changes in body weight (J) of young EP4^{fl/fl} and CD11c^{Cre}EP4^{fl/fl} mice treated with vancomycin and α CD3.

(K–M) Experimental setup (K), changes in body weight (L), and representative recipient terminal ileal histological images (M). Scale bar, 200 μ m.

(N) Relative abundances of SFB and *E. coli* in the recipient ileal contents by qPCR.

(O and P) Representative flow cytometric dot plots and accumulative percentages of siLP T cells (O) and MNP subsets (P).

(B, D, G, H, J, L, and N–P) All data are presented as mean \pm SEM. Numbers in brackets indicate group sizes. Significance is indicated as * p < 0.05, ** p < 0.01, *** p < 0.001, **** p < 0.0001, or ns (not significant).

4. Segal, J.P., Htet, H.M.T., Limdi, J., and Hayee, B. (2020). How to manage IBD in the “elderly.” *Frontline Gastroenterol.* *11*, 468–477. <https://doi.org/10.1136/figastro-2019-101218>.
5. Quin, C., Breznik, J.A., Kennedy, A.E., DeJong, E.N., Andary, C.M., Ermolina, S., Davidson, D.J., Ma, J., Surette, M.G., and Bowdish, D.M. E. (2024). Monocyte-driven inflamm-aging reduces intestinal barrier function in females. *Immun. Ageing* *21*, 65. <https://doi.org/10.1186/s12979-024-00469-6>.
6. De Maeyer, R.P.H., and Chambers, E.S. (2021). The impact of ageing on monocytes and macrophages. *Immunol. Lett.* *230*, 1–10. <https://doi.org/10.1016/j.imlet.2020.12.003>.
7. O’Toole, P.W., and Jeffery, I.B. (2015). Gut microbiota and aging. *Science* *350*, 1214–1215. <https://doi.org/10.1126/science.aac8469>.
8. Wilanski, T., Diener, C., Rappaport, N., Patwardhan, S., Wiedrick, J., Lapidus, J., Earls, J.C., Zimmer, A., Glusman, G., Robinson, M., et al. (2021). Gut microbiome pattern reflects healthy ageing and predicts survival in humans. *Nat. Metab.* *3*, 274–286. <https://doi.org/10.1038/s42255-021-00348-0>.
9. Thevaranjan, N., Puchta, A., Schulz, C., Naidoo, A., Szamosi, J.C., Verschoor, C.P., Loukov, D., Schenck, L.P., Jury, J., Foley, K.P., et al. (2017). Age-Associated Microbial Dysbiosis Promotes Intestinal Permeability, Systemic Inflammation, and Macrophage Dysfunction. *Cell Host Microbe* *21*, 455–466.e4. <https://doi.org/10.1016/j.chom.2017.03.002>.
10. Ivanov, I.I., Tuganbaev, T., Skelly, A.N., and Honda, K. (2022). T Cell Responses to the Microbiota. *Annu. Rev. Immunol.* *40*, 559–587. <https://doi.org/10.1146/annurev-immunol-101320-011829>.
11. Graham, D.B., and Xavier, R.J. (2023). Conditioning of the immune system by the microbiome. *Trends Immunol.* *44*, 499–511. <https://doi.org/10.1016/j.it.2023.05.002>.
12. Yao, C., and Narumiya, S. (2019). Prostaglandin-cytokine crosstalk in chronic inflammation. *Br. J. Pharmacol.* *176*, 337–354. <https://doi.org/10.1111/bph.14530>.
13. Vijay, R., Hua, X., Meyerholz, D.K., Miki, Y., Yamamoto, K., Gelb, M., Murakami, M., and Perlman, S. (2015). Critical role of phospholipase A2 group IID in age-related susceptibility to severe acute respiratory syndrome-CoV infection. *J. Exp. Med.* *212*, 1851–1868. <https://doi.org/10.1084/jem.20150632>.
14. Wong, L.R., Zheng, J., Wilhelmsen, K., Li, K., Ortiz, M.E., Schnicker, N.J., Thurman, A., Pezzulo, A.A., Szachowicz, P.J., Li, P., et al. (2022). Eicosanoid signalling blockade protects middle-aged mice from severe COVID-19. *Nature* *605*, 146–151. <https://doi.org/10.1038/s41586-022-04630-3>.
15. Chen, J., Deng, J.C., Zemans, R.L., Bahmed, K., Kosmider, B., Zhang, M., Peters-Golden, M., and Goldstein, D.R. (2022). Age-induced prostaglandin E2 impairs mitochondrial fitness and increases mortality to influenza infection. *Nat. Commun.* *13*, 6759. <https://doi.org/10.1038/s41467-022-34593-y>.
16. Minhas, P.S., Latif-Hernandez, A., McReynolds, M.R., Durairaj, A.S., Wang, Q., Rubin, A., Joshi, A.U., He, J.Q., Gauba, E., Liu, L., et al. (2021). Restoring metabolism of myeloid cells reverses cognitive decline in ageing. *Nature* *590*, 122–128. <https://doi.org/10.1038/s41586-020-03160-0>.
17. Palla, A.R., Ravichandran, M., Wang, Y.X., Alexandrova, L., Yang, A.V., Kraft, P., Holbrook, C.A., Schürch, C.M., Ho, A.T.V., and Blau, H.M. (2021). Inhibition of prostaglandin-degrading enzyme 15-PGDH rejuvenates aged muscle mass and strength. *Science* *371*, eabc8059. <https://doi.org/10.1126/science.abc8059>.
18. Bakooshli, M.A., Wang, Y.X., Monti, E., Su, S., Kraft, P., Nalbandian, M., Alexandrova, L., Wheeler, J.R., Vogel, H., and Blau, H.M. (2023). Regeneration of neuromuscular synapses after acute and chronic denervation by inhibiting the gerozyme 15-prostaglandin dehydrogenase. *Sci. Transl. Med.* *15*, eadg1485. <https://doi.org/10.1126/scitranslmed.adg1485>.
19. Zhang, Y., Desai, A., Yang, S.Y., Bae, K.B., Antczak, M.I., Fink, S.P., Tiwari, S., Willis, J.E., Williams, N.S., Dawson, D.M., et al. (2015). Inhibition of the Prostaglandin Degrading Enzyme 15-PGDH Potentiates Tissue Regeneration. *Science* *348*, aaa2340. <https://doi.org/10.1126/science.aaa2340>.
20. Duffin, R., O’Connor, R.A., Crittenden, S., Forster, T., Yu, C., Zheng, X., Smyth, D., Robb, C.T., Rossi, F., Skouras, C., et al. (2016). Prostaglandin E₂ constrains systemic inflammation through an innate lymphoid cell-IL-22 axis. *Science* *351*, 1333–1338. <https://doi.org/10.1126/science.aad9903>.
21. Na, Y.R., Jung, D., Stakenborg, M., Jang, H., Gu, G.J., Jeong, M.R., Suh, S.Y., Kim, H.J., Kwon, Y.H., Sung, T.S., et al. (2021). Prostaglandin E2 receptor PTGER4-expressing macrophages promote intestinal epithelial barrier regeneration upon inflammation. *Gut* *70*, 2249–2260. <https://doi.org/10.1136/gutjnl-2020-322146>.
22. Merger, M., Viney, J.L., Borojevic, R., Steele-Norwood, D., Zhou, P., Clark, D.A., Riddell, R., Maric, R., Podack, E.R., and Croitoru, K. (2002). Defining the roles of perforin, Fas/FasL, and tumour necrosis factor alpha in T cell induced mucosal damage in the mouse intestine. *Gut* *51*, 155–163. <https://doi.org/10.1136/gut.51.2.155>.
23. Musch, M.W., Clarke, L.L., Mamah, D., Gawenis, L.R., Zhang, Z., Ellsworth, W., Shalowitz, D., Mittal, N., Efthimiou, P., Alnadjim, Z., et al. (2002). T cell activation causes diarrhea by increasing intestinal permeability and inhibiting epithelial Na⁺/K⁺-ATPase. *J. Clin. Invest.* *110*, 1739–1747. <https://doi.org/10.1172/JCI15695>.
24. Esplugues, E., Huber, S., Gagliani, N., Hauser, A.E., Town, T., Wan, Y.Y., O’Connor, W., Rongvaux, A., Van Rooijen, N., Hagerman, A.M., et al. (2011). Control of TH17 cells occurs in the Small Intestine. *Nature* *475*, 514–518. <https://doi.org/10.1038/nature10228>.
25. Gagliani, N., Amezcua Vesely, M.C.A., Iseppon, A., Brockmann, L., Xu, H., Palm, N.W., de Zoete, M.R., Licona-Limón, P., Paiva, R.S., Ching, T., et al. (2015). Th17 cells transdifferentiate into regulatory T cells during resolution of inflammation. *Nature* *523*, 221–225. <https://doi.org/10.1038/nature14452>.
26. Caronni, N., La Terza, F., Vittoria, F.M., Barbiera, G., Mezzanzanica, L., Cuzzola, V., Barresi, S., Pellegatta, M., Canevazzi, P., Dunsmore, G., et al. (2023). IL-1β⁺ macrophages fuel pathogenic inflammation in pancreatic cancer. *Nature* *623*, 415–422. <https://doi.org/10.1038/s41586-023-06685-2>.
27. Hajeyah, A.A., Griffiths, W.J., Wang, Y., Finch, A.J., and O’Donnell, V.B. (2020). The Biosynthesis of Enzymatically Oxidized Lipids. *Front. Endocrinol. (Lausanne)* *11*, 591819. <https://doi.org/10.3389/fendo.2020.591819>.
28. Arijis, I., De Hertogh, G., Lemaire, K., Quintens, R., Van Lommel, L., Van Steen, K., Leemans, P., Cleynen, I., Van Assche, G., Vermeire, S., et al. (2009). Mucosal gene expression of antimicrobial peptides in inflammatory bowel disease before and after first infliximab treatment. *PLoS One* *4*, e7984. <https://doi.org/10.1371/journal.pone.0007984>.
29. Martin, J.C., Chang, C., Boschetti, G., Ungaro, R., Giri, M., Grout, J.A., Gettler, K., Chuang, L.S., Nayar, S., Greenstein, A.J., et al. (2019). Single-Cell Analysis of Crohn’s Disease Lesions Identifies a Pathogenic Cellular Module Associated with Resistance to Anti-TNF Therapy. *Cell* *178*, 1493–1508.e20. <https://doi.org/10.1016/j.cell.2019.08.008>.
30. Thomas, M.F., Slowikowski, K., Manakongtreecheep, K., Sen, P., Samanta, N., Tantivit, J., Nasrallah, M., Zubiri, L., Smith, N.P., Tirard, A., et al. (2024). Single-cell transcriptomic analyses reveal distinct immune cell contributions to epithelial barrier dysfunction in checkpoint inhibitor colitis. *Nat. Med.* *30*, 1349–1362. <https://doi.org/10.1038/s41591-024-02895-x>.
31. Zhou, Y., Medik, Y.B., Patel, B., Zamlar, D.B., Chen, S., Chapman, T., Schneider, S., Park, E.M., Babcock, R.L., Chrisikos, T.T., et al. (2023). Intestinal toxicity to CTLA-4 blockade driven by IL-6 and myeloid infiltration. *J. Exp. Med.* *220*, e20221333. <https://doi.org/10.1084/jem.20221333>.

32. Crittenden, S., Goepf, M., Pollock, J., Robb, C.T., Smyth, D.J., Zhou, Y., Andrews, R., Tyrrell, V., Gkikas, K., Adima, A., et al. (2021). Prostaglandin E2 promotes intestinal inflammation via inhibiting microbiota-dependent regulatory T cells. *Sci. Adv.* 7, eabd7954. <https://doi.org/10.1126/sciadv.abd7954>.
33. Ushikubi, F., Segi, E., Sugimoto, Y., Murata, T., Matsuoka, T., Kobayashi, T., Hizaki, H., Tuboi, K., Katsuyama, M., Ichikawa, A., et al. (1998). Impaired febrile response in mice lacking the prostaglandin E receptor subtype EP3. *Nature* 395, 281–284. <https://doi.org/10.1038/26233>.
34. Segi, E., Sugimoto, Y., Yamasaki, A., Aze, Y., Oida, H., Nishimura, T., Murata, T., Matsuoka, T., Ushikubi, F., Hirose, M., et al. (1998). Patent ductus arteriosus and neonatal death in prostaglandin receptor EP4-deficient mice. *Biochem. Biophys. Res. Commun.* 246, 7–12. <https://doi.org/10.1006/bbrc.1998.8461>.
35. Hiromi, T., Yokoyama, U., Kurotaki, D., Mamun, A., Ishiwata, R., Ichikawa, Y., Nishihara, H., Umemura, M., Fujita, T., Yasuda, S., et al. (2020). Excessive EP4 Signaling in Smooth Muscle Cells Induces Abdominal Aortic Aneurysm by Amplifying Inflammation. *Arterioscler. Thromb. Vasc. Biol.* 40, 1559–1573. <https://doi.org/10.1161/ATVBAHA.120.314297>.
36. Yao, C., Hirata, T., Soontrapa, K., Ma, X., Takemori, H., and Narumiya, S. (2013). Prostaglandin E₂ promotes Th1 differentiation via synergistic amplification of IL-12 signalling by cAMP and PI3-kinase. *Nat. Commun.* 4, 1685. <https://doi.org/10.1038/ncomms2684>.
37. Lee, J., Aoki, T., Thumkeo, D., Siritwach, R., Yao, C., and Narumiya, S. (2019). T cell-intrinsic prostaglandin E2-EP2/EP4 signaling is critical in pathogenic TH17 cell-driven inflammation. *J. Allergy Clin. Immunol.* 143, 631–643. <https://doi.org/10.1016/j.jaci.2018.05.036>.
38. Robb, C.T., McSorley, H.J., Lee, J., Aoki, T., Yu, C., Crittenden, S., Astier, A., Felton, J.M., Parkinson, N., Ayele, A., et al. (2018). Prostaglandin E2 stimulates adaptive IL-22 production and promotes allergic contact dermatitis. *J. Allergy Clin. Immunol.* 141, 152–162. <https://doi.org/10.1016/j.jaci.2017.04.045>.
39. Schneider, A., Guan, Y., Zhang, Y., Magnuson, M.A., Pettepher, C., Loftin, C.D., Langenbach, R., Breyer, R.M., and Breyer, M.D. (2004). Generation of a conditional allele of the mouse prostaglandin EP4 receptor. *Genesis* 40, 7–14. <https://doi.org/10.1002/gene.20048>.
40. Nizzoli, G., Burrello, C., Cribiù, F.M., Lovati, G., Ercoli, G., Botti, F., Trombetta, E., Porretti, L., Todoerti, K., Neri, A., et al. (2018). Pathogenicity of In Vivo Generated Intestinal Th17 Lymphocytes is IFN γ Dependent. *J. Crohns Colitis* 12, 981–992. <https://doi.org/10.1093/ecco-jcc/jjy051>.
41. Harbour, S.N., Maynard, C.L., Zindl, C.L., Schoeb, T.R., and Weaver, C.T. (2015). Th17 cells give rise to Th1 cells that are required for the pathogenesis of colitis. *Proc. Natl. Acad. Sci. USA* 112, 7061–7066. <https://doi.org/10.1073/pnas.1415675112>.
42. Stranges, P.B., Watson, J., Cooper, C.J., Choisy-Rossi, C.-M., Stonebraker, A.C., Beighton, R.A., Hartig, H., Sundberg, J.P., Servick, S., Kaufmann, G., et al. (2007). Elimination of antigen-presenting cells and autoreactive T cells by Fas contributes to prevention of autoimmunity. *Immunity* 26, 629–641. <https://doi.org/10.1016/j.immuni.2007.03.016>.
43. Chou, W.-L., Chuang, L.-M., Chou, C.-C., Wang, A.H.-J., Lawson, J.A., FitzGerald, G.A., and Chang, Z.-F. (2007). Identification of a novel prostaglandin reductase reveals the involvement of prostaglandin E2 catabolism in regulation of peroxisome proliferator-activated receptor gamma activation. *J. Biol. Chem.* 282, 18162–18172. <https://doi.org/10.1074/jbc.M702289200>.
44. Hazra, S., Peebles, K.A., Sharma, S., Mao, J.T., and Dubinett, S.M. (2008). The Role of PPAR γ in the Cyclooxygenase Pathway in Lung Cancer. *PPAR Res.* 2008, 790568. <https://doi.org/10.1155/2008/790568>.
45. Nelson, V.L., Nguyen, H.C.B., Garcia-Cañaveras, J.C., Briggs, E.R., Ho, W.Y., DiSpirito, J.R., Marinis, J.M., Hill, D.A., and Lazar, M.A. (2018). PPAR γ is a nexus controlling alternative activation of macrophages via glutamine metabolism. *Genes Dev.* 32, 1035–1044. <https://doi.org/10.1101/gad.312355.118>.
46. Byndloss, M.X., Olsan, E.E., Rivera-Chávez, F., Tiffany, C.R., Cevallos, S.A., Lokken, K.L., Torres, T.P., Byndloss, A.J., Faber, F., Gao, Y., et al. (2017). Microbiota-activated PPAR- γ signaling inhibits dysbiotic Enterobacteriaceae expansion. *Science* 357, 570–575. <https://doi.org/10.1126/science.aam9949>.
47. Shah, Y.M., Morimura, K., and Gonzalez, F.J. (2007). Expression of peroxisome proliferator-activated receptor-gamma in macrophage suppresses experimentally induced colitis. *Am. J. Physiol. Gastrointest. Liver Physiol.* 292, G657–G666. <https://doi.org/10.1152/ajpgi.00381.2006>.
48. Ladinsky, M.S., Araujo, L.P., Zhang, X., Veltri, J., Galan-Diez, M., Soualhi, S., Lee, C., Irie, K., Pinker, E.Y., Narushima, S., et al. (2019). Endocytosis of commensal antigens by intestinal epithelial cells regulates mucosal T cell homeostasis. *Science* 363. <https://doi.org/10.1126/science.aat4042>.
49. Ivanov, I.I., Atarashi, K., Manel, N., Brodie, E.L., Shima, T., Karaoz, U., Wei, D., Goldfarb, K.C., Santee, C.A., Lynch, S.V., et al. (2009). Induction of intestinal Th17 cells by segmented filamentous bacteria. *Cell* 139, 485–498. <https://doi.org/10.1016/j.cell.2009.09.033>.
50. Gaboriau-Routhiau, V., Rakotobe, S., Lécuycer, E., Mulder, I., Lan, A., Bridonneau, C., Rochet, V., Pisi, A., De Paepe, M., Brandi, G., et al. (2009). The key role of segmented filamentous bacteria in the coordinated maturation of gut helper T cell responses. *Immunity* 31, 677–689. <https://doi.org/10.1016/j.immuni.2009.08.020>.
51. Omenetti, S., Bussi, C., Metidji, A., Iseppon, A., Lee, S., Tolaini, M., Li, Y., Kelly, G., Chakravarty, P., Shoaie, S., et al. (2019). The Intestine Harbors Functionally Distinct Homeostatic Tissue-Resident and Inflammatory Th17 Cells. *Immunity* 51, 77–89.e6. <https://doi.org/10.1016/j.immuni.2019.05.004>.
52. Kawano, Y., Edwards, M., Huang, Y., Bilate, A.M., Araujo, L.P., Tanoue, T., Atarashi, K., Ladinsky, M.S., Reiner, S.L., Wang, H.H., et al. (2022). Microbiota imbalance induced by dietary sugar disrupts immune-mediated protection from metabolic syndrome. *Cell* 185, 3501–3519.e20. <https://doi.org/10.1016/j.cell.2022.08.005>.
53. Brockmann, L., Tran, A., Huang, Y., Edwards, M., Ronda, C., Wang, H.H., and Ivanov, I.I. (2023). Intestinal microbiota-specific Th17 cells possess regulatory properties and suppress effector T cells via c-MAF and IL-10. *Immunity* 56, 2719–2735.e7. <https://doi.org/10.1016/j.immuni.2023.11.003>.
54. Tuganbaev, T., Mor, U., Bashiardes, S., Liwinski, T., Nobs, S.P., Leshem, A., Dori-Bachash, M., Thaiss, C.A., Pinker, E.Y., Ratiner, K., et al. (2020). Diet Diurnally Regulates Small Intestinal Microbiome-Epithelial-Immune Homeostasis and Enteritis. *Cell* 182, 1441–1459.e21. <https://doi.org/10.1016/j.cell.2020.08.027>.
55. Lai, N.Y., Musser, M.A., Pinho-Ribeiro, F.A., Baral, P., Jacobson, A., Ma, P., Potts, D.E., Chen, Z., Paik, D., Soualhi, S., et al. (2020). Gut-Innervating Nociceptor Neurons Regulate Peyer's Patch Microfold Cells and SFB Levels to Mediate Salmonella Host Defense. *Cell* 180, 33–49.e22. <https://doi.org/10.1016/j.cell.2019.11.014>.
56. Bolsega, S., Basic, M., Smoczek, A., Buettner, M., Eberl, C., Ahrens, D., Odum, K.A., Stecher, B., and Bleich, A. (2019). Composition of the Intestinal Microbiota Determines the Outcome of Virus-Triggered Colitis in Mice. *Front. Immunol.* 10, 1708. <https://doi.org/10.3389/fimmu.2019.01708>.
57. Yang, K., Li, J., Sun, Z., Bai, C., and Zhao, L. (2023). Effect of age on the risk of immune-related adverse events in patients receiving immune checkpoint inhibitors. *Clin. Exp. Med.* 23, 3907–3918. <https://doi.org/10.1007/s10238-023-01055-8>.
58. Sendama, W. (2020). The effect of ageing on the resolution of inflammation. *Ageing Res. Rev.* 57, 101000. <https://doi.org/10.1016/j.arr.2019.101000>.
59. Hong, S.J., Galati, J., and Katz, S. (2022). Crohn's Disease of the Elderly: Unique Biology and Therapeutic Efficacy and Safety. *Gastroenterol. Clin. North Am.* 51, 425–440. <https://doi.org/10.1016/j.gtc.2021.12.014>.
60. Taleban, S., Colombel, J.-F., Mohler, M.J., and Fain, M.J. (2015). Inflammatory bowel disease and the elderly: a review. *J. Crohns Colitis* 9, 507–515. <https://doi.org/10.1093/ecco-jcc/jjv059>.

61. Johnson, A.M.F., Costanzo, A., Gareau, M.G., Armando, A.M., Quehenberger, O., Jameson, J.M., and Olefsky, J.M. (2015). High fat diet causes depletion of intestinal eosinophils associated with intestinal permeability. *PLoS One* *10*, e0122195. <https://doi.org/10.1371/journal.pone.0122195>.
62. Lee, J.-Y., Cevallos, S.A., Byndloss, M.X., Tiffany, C.R., Olsan, E.E., Butler, B.P., Young, B.M., Rogers, A.W.L., Nguyen, H., Kim, K., et al. (2020). High-Fat Diet and Antibiotics Cooperatively Impair Mitochondrial Bioenergetics to Trigger Dysbiosis that Exacerbates Pre-inflammatory Bowel Disease. *Cell Host Microbe* *28*, 273–284.e6. <https://doi.org/10.1016/j.chom.2020.06.001>.
63. Hohman, L.S., and Osborne, L.C. (2022). A gut-centric view of aging: Do intestinal epithelial cells contribute to age-associated microbiota changes, inflammaging, and immunosenescence? *Aging Cell* *21*, e13700. <https://doi.org/10.1111/ace1.13700>.
64. Leite, G., Pimentel, M., Barlow, G.M., Chang, C., Hosseini, A., Wang, J., Parodi, G., Sedighi, R., Rezaie, A., and Mathur, R. (2021). Age and the aging process significantly alter the small bowel microbiome. *Cell Rep.* *36*, 109765. <https://doi.org/10.1016/j.celrep.2021.109765>.
65. Bradley, E., and Haran, J. (2024). The human gut microbiome and aging. *Gut Microbes* *16*, 2359677. <https://doi.org/10.1080/19490976.2024.2359677>.
66. Ghosh, T.S., Shanahan, F., and O'Toole, P.W. (2022). The gut microbiome as a modulator of healthy ageing. *Nat. Rev. Gastroenterol. Hepatol.* *19*, 565–584. <https://doi.org/10.1038/s41575-022-00605-x>.
67. Pittayanon, R., Lau, J.T., Leontiadis, G.I., Tse, F., Yuan, Y., Surette, M., and Moayyedi, P. (2020). Differences in Gut Microbiota in Patients With vs Without Inflammatory Bowel Diseases: A Systematic Review. *Gastroenterology* *158*, 930–946.e1. <https://doi.org/10.1053/j.gastro.2019.11.294>.
68. Heczko, U., Abe, A., and Finlay, B.B. (2000). Segmented filamentous bacteria prevent colonization of enteropathogenic *Escherichia coli* O103 in rabbits. *J. Infect. Dis.* *181*, 1027–1033. <https://doi.org/10.1086/315348>.
69. Subramanian, A., Tamayo, P., Mootha, V.K., Mukherjee, S., Ebert, B.L., Gillette, M.A., Paulovich, A., Pomeroy, S.L., Golub, T.R., Lander, E.S., et al. (2005). Gene set enrichment analysis: a knowledge-based approach for interpreting genome-wide expression profiles. *Proc. Natl. Acad. Sci. USA* *102*, 15545–15550. <https://doi.org/10.1073/pnas.0506580102>.
70. Callahan, B.J., McMurdie, P.J., Rosen, M.J., Han, A.W., Johnson, A.J.A., and Holmes, S.P. (2016). DADA2: High-resolution sample inference from Illumina amplicon data. *Nat. Methods* *13*, 581–583. <https://doi.org/10.1038/nmeth.3869>.
71. McMurdie, P.J., and Holmes, S. (2013). phyloseq: an R package for reproducible interactive analysis and graphics of microbiome census data. *PLoS One* *8*, e61217. <https://doi.org/10.1371/journal.pone.0061217>.
72. Ewels, P., Magnusson, M., Lundin, S., and Källner, M. (2016). MultiQC: summarize analysis results for multiple tools and samples in a single report. *Bioinformatics* *32*, 3047–3048. <https://doi.org/10.1093/bioinformatics/btw354>.
73. Chen, S., Zhou, Y., Chen, Y., and Gu, J. (2018). fastp: an ultra-fast all-in-one FASTQ preprocessor. *Bioinformatics* *34*, i884–i890. <https://doi.org/10.1093/bioinformatics/bty560>.
74. Li, H. (2013). Aligning sequence reads, clone sequences and assembly contigs with BWA-MEM. Preprint at arXiv. <https://doi.org/10.48550/arXiv.1303.3997>.
75. Li, H., Handsaker, B., Wysoker, A., Fennell, T., Ruan, J., Homer, N., Marth, G., Abecasis, G., and Durbin, R.; 1000 Genome Project Data Processing Subgroup (2009). The Sequence Alignment/Map format and SAMtools. *Bioinformatics* *25*, 2078–2079. <https://doi.org/10.1093/bioinformatics/btp352>.
76. Blanco-Míguez, A., Beghini, F., Cumbo, F., McIver, L.J., Thompson, K.N., Zolfo, M., Manghi, P., Dubois, L., Huang, K.D., Thomas, A.M., et al. (2023). Extending and improving metagenomic taxonomic profiling with uncharacterized species using MetaPhlan 4. *Nat. Biotechnol.* *41*, 1633–1644. <https://doi.org/10.1038/s41587-023-01688-w>.
77. Dixon, P. (2003). VEGAN, a package of R functions for community ecology. *J. Veg. Sci.* *14*, 927–930. <https://doi.org/10.1111/j.1654-1103.2003.tb02228.x>.
78. Noble, C.L., Abbas, A.R., Lees, C.W., Cornelius, J., Toy, K., Modrusan, Z., Clark, H.F., Arnott, I.D., Penman, I.D., Satsangi, J., et al. (2010). Characterization of intestinal gene expression profiles in Crohn's disease by genome-wide microarray analysis. *Inflamm. Bowel Dis.* *16*, 1717–1728. <https://doi.org/10.1002/ibd.21263>.

STAR★METHODS

KEY RESOURCES TABLE

REAGENT or RESOURCE	SOURCE	IDENTIFIER
Antibodies		
<i>InVivo</i> MAB polyclonal Armenian hamster IgG	BioXCell	Cat#BE0091; RRID:AB_1107773
<i>InVivo</i> MAB anti-mouse CD3 ϵ (clone 145-2C11)	BioXCell	Cat#BE0001; RRID:AB_2714218
<i>InVivo</i> MAB anti-mouse CD3 (clone 17A2)	BioXCell	Cat#BE0002; RRID:AB_1107630
CD45 Monoclonal Antibody (30-F11), eFluor™ 450, eBioscience™	ThermoFisher Scientific	Cat#48-0451-82; RRID:AB_1518806
CD3 ϵ Monoclonal Antibody (145-2C11), PE, eBioscience™	ThermoFisher Scientific	Cat#12-0031-82; RRID:AB_465496
CD3 ϵ Monoclonal Antibody (eBio500A2 (500A2)), Alexa Fluor™ 700, eBioscience™	ThermoFisher Scientific	Cat#56-0033-82; RRID:AB_837094
Brilliant Violet 650™ anti-mouse CD4 Antibody (clone RM4-5)	BioLegend	Cat#100545; RRID:AB_11126142
Brilliant Violet 510™ anti-mouse CD8a Antibody (clone 53-6.7)	BioLegend	Cat#100752; RRID:AB_2563057
FITC anti-mouse/human CD11b Antibody (clone M1/70)	BioLegend	Cat#101206; RRID:AB_312789
Brilliant Violet 605™ anti-mouse Ki-67 Antibody (clone 16A8)	BioLegend	Cat#652413; RRID:AB_2562664
FITC anti-mouse CD11c Antibody (clone N418)	BioLegend	Cat#117306; RRID:AB_312789
CD25 Monoclonal Antibody (PC61.5), APC, eBioscience™	ThermoFisher Scientific	Cat#17-0251-82; RRID:AB_469366
CD11c Monoclonal Antibody (N418), APC	ThermoFisher Scientific	Cat#17-0114-82; RRID:AB_469346
CD11b Monoclonal Antibody (M1/70), APC, eBioscience™	ThermoFisher Scientific	Cat#17-0112-82; RRID:AB_469343
IL-17A Monoclonal Antibody (eBio17B7), PerCP-Cyanine5	ThermoFisher Scientific	Cat#45-7177-82; RRID:AB_925753
IFN gamma Monoclonal Antibody (XMG1.2), PE	ThermoFisher Scientific	Cat#12-7311-82; RRID:AB_466193
FOXP3 Monoclonal Antibody (FJK-16s), FITC	ThermoFisher Scientific	Cat#11-5773-82; RRID:11-5773-82
FOXP3 Monoclonal Antibody (FJK-16s), PE	ThermoFisher Scientific	Cat#12-5773-82; RRID:AB_465936
ROR gamma (t) Monoclonal Antibody (B2D), PerCP-eFluor™ 710, eBioscience™	ThermoFisher Scientific	Cat#46-6981-82; RRID:AB_10717956
APC anti-T-bet Antibody (4B10)	BioLegend	Cat#644814; RRID:AB_10901173
Alexa Fluor® 700 anti-mouse I-A/I-E Antibody (clone M5/114.15.2)	BioLegend	Cat#107622; RRID:AB_493727
PE/Cyanine7 anti-mouse Ly-6G Antibody (1A8)	BioLegend	Cat#127618; RRID:AB_1877261
Brilliant Violet 785™ anti-mouse Ly-6C Antibody (HK1.4)	BioLegend	Cat#128041; RRID:AB_2565852
PerCP/Cyanine5.5 anti-mouse CD64 (Fc γ R1) Antibody (X54-5/7.1)	BioLegend	Cat#139308; RRID:AB_2561963
APC anti-mouse CD24 Antibody (clone M1/69)	BioLegend	Cat#101813; RRID:AB_439715
APC anti-mouse CD80 Antibody (16-10A1)	BioLegend	Cat#104714; RRID:AB_313135
PE/Cyanine7 anti-mouse CD86 Antibody (PO3)	BioLegend	Cat#105116; RRID:AB_493600
Brilliant Violet 605™ anti-mouse CD206 (MMR) Antibody (C068C2)	BioLegend	Cat#141721; RRID:AB_2562340
PPAR γ (81B8) Rabbit mAb	Cell Signaling Technology	Cat#2443S; RRID:AB_823598
Normal rabbit IgG	Cell Signaling Technology	Cat#2729; RRID:AB_1031062
Anti-rabbit IgG (H+L), F(ab') ₂ Fragment (Alexa Fluor® 594 Conjugate)	Cell Signaling Technology	Cat#8889S
Bacterial and virus strains		
GF intestinal contents	Bolsega et al. ⁵²	N/A
SFB-monoassociated intestinal contents	Bolsega et al. ⁵²	N/A
Chemicals, peptides, and recombinant proteins		
DMSO	ThermoFisher Scientific	85190
Indomethacin	Sigma-Aldrich	I7378

(Continued on next page)

Continued

REAGENT or RESOURCE	SOURCE	IDENTIFIER
Prostaglandin E ₂	Cayman	14010
L-902,688	Cayman	10007712
L-161,982	Abcam	Ab120947
Rosiglitazone	Abcam	Ab142461
Ampicillin Sodium Salt	Fisher Scientific	10193433
Gentamycin	Sigma	G3632-5G
Metronidazole	Sigma	M1547
Neomycin	Sigma	N1876
Vancomycin	Enzo Life	ALX-380-279-G001
Sucralose	Sigma	69293
Mouse GM-CSF	Miltenyi Biotec	130-094-043
RPMI 1640	Gibco	11875093
HBSS	Gibco	14175
DNase I	Sigma-Aldrich	DN-25-1G
Collagenase IV	Life Technologies	17104019
EDTA	Fisher Scientific	BP2482
Phorbol 12-myristate 13-acetate	Merck Life Sciences	P8139
Ionomycin calcium salt	Merck Life Sciences	I0634

Critical commercial assays

BD Cytofix/Cytoperm Fixation/Permeabilization Kit	BD Biosciences	554714
Foxp3/Transcription Factor Fix and Staining Buffer set	ThermoFisher Scientific	00-5523-00
Chromium Single Cell 3' Library Kit v3.1	10X Genomics	PN-1000268
NextSeq 1000/2000 P3 Reagents v3 Kit	Illumina	20100983
DNeasy PowerLyzer PowerSoil Kit	Qiagen	12855
RNeasy Mini Kit	Qiagen	74104
High Capacity cDNA Reverse Transcription Kit	ThermoFisher Scientific	4368814
GoTaq® qPCR Master Mix	Promega	A6002

Deposited data

Mouse small intestinal single immune cell RNA sequencing data	NCBI Sequencing Read Archive	PRJNA1109827
Mouse ileal bulk RNA sequencing data	NCBI Sequencing Read Archive	PRJNA978526
Mouse ileal microbial 16S sequencing data	NCBI Sequencing Read Archive	PRJNA972542
Mouse ileal microbial shotgun metagenomic sequencing data	European Nucleotide Archive	PRJEB83270

Experimental models: Organisms/strains

Mouse: C57BL/6J0laHsd	Harlan UK	N/A
Mouse: C57BL/6Ncrl	Charles River UK	N/A
Mouse: B6(Cg)-Tyr ^{c-2} /J (B6 Albino)	Charles River UK	JAX 000058
Mouse: B6.129-Ptger2 ^{tm1Sna} (EP2KO)	Ushikubi et al. ³³	CARD: 1992
Mouse: B6.129-Ptger4 ^{tm1Sna} (EP4KO)	Segi et al. ³⁴	CARD: 2035
Mouse: B6.129S6(D2)-Ptger4 ^{tm1.1Matb} /BreyJ (EP4 ^{fl/fl})	The Jackson Laboratory	JAX: 028102
Mouse: C57BL/6J-Tg(ltgax-cre,-EGFP)4097Ach/J	The Jackson Laboratory	JAX: 007567
Mouse: Lck ^{Cre} EP4 ^{fl/fl}	Crittenden et al. ³¹	N/A
Mouse: CD11c ^{Cre} EP4 ^{fl/fl}	Crittenden et al. ³¹	N/A

Oligonucleotides

Information regarding oligonucleotides used in this study is listed in [Table S1](#)

Software and algorithms

Flowjo v8, v9, v10	BD Biosciences	https://www.flowjo.com
Prism v10	Graphpad	https://www.graphpad.com

(Continued on next page)

Continued

REAGENT or RESOURCE	SOURCE	IDENTIFIER
Trailmaker™ scRNA-seq data analysis platform	Parse Biosciences	https://www.parsebiosciences.com/data-analysis/
R version 4	R Project for Statistical Computing	https://www.r-project.org

EXPERIMENTAL MODEL AND STUDY PARTICIPANT DETAILS

Animal Experiments

All experiments were conducted in accordance with the UK Scientific Procedures Act of 1986 and had local ethical approval from the University of Edinburgh Animal Welfare and Ethical Review Body.

EP2KO,³³ EP4KO,³⁴ EP4-floxed,³⁹ and CD11c-Cre-EGFP⁴² mice were bred and maintained under specific pathogen-free (SPF) conditions in accredited animal facilities at the University of Edinburgh. EP4-floxed mice were crossed to Lck-Cre or CD11c-Cre-GFP mice to generate T- or MNP-specific EP4-deficient mice (i.e., Lck^{Cre}EP4^{fl/fl} or CD11c^{Cre}EP4^{fl/fl}), respectively.³² Young and middle-aged wild-type C57BL/6 and B6 Albino mice were bred in the animal facilities at the University of Edinburgh or purchased from Harlan UK or Charles River UK. Mice were aged >8 weeks old at the beginning of use and sex- and age-matched. Middle-aged (11–15 months old) mice are used as indicated in the text and figure legends. Both male and female mice were used in experiments, and no sex differences were observed in our models. Mice were selected based on their genotype and age, with littermate controls used when feasible. Given the limitations in litter sizes, multiple litters from independent experiments were pooled to ensure robust sample sizes for effective statistical analysis. Mice were analyzed individually and no mice were excluded from the analysis, with the exception of exclusions due to technical errors in misinjection or isolation of single intestinal lamina propria immune cells.

Mice were injected intraperitoneally (i.p.) with 20 µg per injection of anti-mouse CD3ε monoclonal antibody (αCD3, clone 145-2C11, BioXCell) or IgG control on day 0 or indicated time points as shown in respective figure legends, while mice represented in Figure 3K were administered αCD3 (clone 17A2, BioXCell). Throughout the experimental timeline, mice were weighed daily, and animals were humanely culled if either their weight loss was greater than 20%.

When indicated, mice were treated with indomethacin (5 mg per kg body weight per day, Sigma) or vehicle control (0.5% EtOH) in drinking water or via i.p. injections as indicated. In some experiments, mice were treated by i.p. injection with an EP4 selective agonist (L-902,688, Cayman) at the dose of 10 µg per injection per day. As indicated, mice were treated with an EP4 selective antagonist (L-161,982 from Abcam, 20 mg per kg body weight per day) or vehicle control (0.5% DMSO) in drinking water for periods indicated in the figure legends. The PPAR_γ agonist, rosiglitazone (Abcam, 20 mg per kg body weight per day), was injected i.p. daily from a week before αCD3 injection and throughout the experiment.

In Figure 7A, recipient SPF WT C57BL/6 mice were pre-treated with a cocktail of antibiotics containing ampicillin (0.5 mg/ml), gentamycin (0.5 mg/ml), metronidazole (0.5 mg/ml), neomycin (0.5 mg/ml), vancomycin (0.25 mg/ml) plus sucralose (4 mg/ml) in drinking water for 2 weeks. After discontinuing antibiotics, animals were rested for 2 days and then administered with fresh cecal microbiota collected from naïve SPF EP4^{fl/fl} or CD11c^{Cre}EP4^{fl/fl} mice through oral gavage as indicated. The recipient mice were then injected i.p. with αCD3. In Figures 7F, 7I, and 7K, recipient SPF C57BL/6 mice were pretreated with vancomycin (0.5 mg/ml) plus sucralose (4 mg/ml) in drinking water for indicated periods. Sucralose (4 mg/ml) was added in the drinking water as vehicle control. In Figure 7K, mice were rested for one day with normal water after withdrawal of vancomycin, then recipient mice received gut contents from SFB-monocolonized mice or from germ-free mice as negative control through oral gavage on two consecutive days. On 14 days after first oral gavage of SFB gut contents, mice were injected i.p. with αCD3 and terminated 3 days later. In Figure 4H, SPF EP4^{fl/fl} and CD11c^{Cre}EP4^{fl/fl} mice were co-housed for more than 4 weeks before αCD3 injection.

Bone marrow-derived MNP culture

Bone marrow cells were flushed from mouse femurs, and cultured with GM-CSF (20 ng/ml) in complete RPMI1640 for 6–7 days. Live CD11c⁺CD11b⁺F4/80⁺ cells were FACS sorted and further cultured with GM-CSF in the presence of PGE₂ (100 nM, Cayman) or EP4 agonist (L-902,688, 100 nM) overnight. Cells were then stained for analysis using flow cytometry.

METHOD DETAILS

Intestinal histology

Terminal ileum samples were fixed with 10% neutral buffered formalin solution (Sigma), embedded in paraffin, and 5 µm sections were used for staining with hematoxylin and eosin (H&E) or Alcian blue/periodic acid–Schiff (AB-PAS). Histology images were taken by Axioscan slide scanners (Zeiss).

Isolation of intestinal lamina propria cells

Intestinal lamina propria (LP) cells were isolated as described previously.²⁰ In brief, mice were culled and their intestines removed and placed in cold PBS. After removing any remaining fatty and mesenteric tissues, samples were cut open longitudinally and any

contents removed before being washed with HBSS buffer containing 2% FCS, and then cut into 0.5 cm pieces. Intestines were shaken at 37°C for 15 min in HBSS containing 2 mM EDTA. After washing with pre-warmed HBSS buffer, intestines were again shaken at 37°C for 30 min in HBSS containing 2 mM EDTA followed by a wash with HBSS. Intestines were then transferred into gentleMACS C tubes (Miltenyi) digested in RPMI 1640 medium containing 10% FCS, 1% L-glutamine and antibiotics with 1.25 mg/ml collagenase IV and 30 µg/ml DNase-I by shaking at 37°C for 30 min. Digested tissues were homogenized by the gentleMACS dissociator running the programme m_intestine_01 and then mashed through a cell strainer and flushed through with HBSS containing 2% FCS. After centrifugation, cells were resuspended in complete RPMI 1640 medium for counting, staining, culture and/or sorting.

Surface and intracellular staining

For surface staining, cells were firstly stained with the Fixable Viability Dye eFluor® 780 (eBioscience) on ice for 30 min to exclude dead cells. After washing with staining buffer, cells were stained on ice for another 30 min with the indicated Abs. For intracellular staining of cytokines, cells were re-stimulated with PMA (50 ng/ml, Sigma) and Ionomycin (500 ng/ml, Sigma) for 3–4 h in the presence of GolgiPlug (BD Bioscience). After staining with the Fixable Viability Dye eFluor® 780 and surface markers, cells were fixed using BD Cytotfix/Cytoperm Fixation buffer (BD Bioscience) for 30 min and then stained with Abs against mouse IFN- γ and IL-17A in the BD Perm/Wash Buffer on ice for 30 min. For intracellular staining of transcription factors, a Foxp3/Transcription Factor Fix and Staining Buffer (eBioscience) and Abs against mouse Ki-67, Foxp3, T-bet, and ROR- γ t were used. To stain PPAR γ , cells were fixed by a Foxp3/Transcription Factor Fix buffer (eBioscience) for >2 h followed by staining for surface markers and an anti-PPAR γ Rabbit mAb (clone D1G6, Cell Signaling) or a normal rabbit IgG for 1 h. After washing, cells were incubated with Alexa Fluor 594 anti-Rabbit IgG for another 30 min. Flow cytometry was performed on the BD LSRFortessa (BD Bioscience) and analyzed by FlowJo software (Tree Star).

Oxylin analysis

Small intestine samples were weighed and homogenized with ceramic beads in 1 mL anti-oxidation buffer containing 100 µM diethylenetriaminepentaacetic acid (DTPA) and 100 µM butylated hydroxytoluene (BHT) in phosphate buffered saline using a Bead Ruptor Elite for 2 x 30 second intervals at 6 m/s, under cooled nitrogen gas (4°C). Samples were spiked with 2.1–2.9 ng of PGE₂-d4, PGD₂-d4, PGF_{2 α} -d4, TXB₂-d4 standards (Cayman Chemical) prior to homogenization. Lipids were extracted by adding a 2.5 ml solvent mixture (1 M acetic acid/isopropanol/hexane; 2:20:30, v/v/v) to 1 ml tissue homogenates in a glass extraction vial and vortexed for 30 sec. 2.5 ml hexane was added to samples and after vortexing for 30 seconds, tubes were centrifuged (500 g for 5 min at 4°C) to recover lipids in the upper hexane layer (aqueous phase), which was transferred to a clean tube. Aqueous samples were re-extracted as above by addition of 2.5 ml hexane, and upper layers were combined. Lipid extraction from the lower aqueous layer was then completed according to the Bligh and Dyer technique using sequential additions of methanol, chloroform and water, and the lower layer was recovered following centrifugation as above and combined with the upper layers from the first stage of extraction. Solvent was dried under vacuum and lipid extract was reconstituted in 200 µl HPLC grade methanol. Lipids were separated by liquid chromatography (LC) using a gradient of 30–100% B over 20 minutes (A: Water:Mob B 95:5 + 0.1% Acetic Acid, B: Acetonitrile: Methanol – 80:15 + 0.1% Acetic Acid) on an Eclipse Plus C18 Column (Agilent), and analysed on a Sciex QTRAP® 7500 LC-MS/MS system. Source conditions: TEM 475°C, IS -2500, GS1 40, GS2 60, CUR 40. Lipids were detected using MRM monitoring with the following parent to daughter ion transitions: PGD₁ and PGE₁ [M-H]⁻ 353.2/317.2, PGD₂, 8-iso PGE₂ and PGE₂ [M-H]⁻ 351.2/271.1, PGF_{2 α} [M-H]⁻ 353.2/309.2, 6-keto PGF_{1 α} [M-H]⁻ 369.2/163.1, TXB₂ [M-H]⁻ 369.2/169.1, 13,14-dihydro-15-keto-PGE₂ [M-H]⁻ 351.2/235.1. Deuterated internal standards were monitored using parent to daughter ions transitions of: TXB₂-d4 [M-H]⁻ 373.2/173.1, PGE₂-d4 and PGD₂-d4 [M-H]⁻ 355.2/275.1, PGF_{2 α} -d4 [M-H]⁻ 357.5/313.2. Chromatographic peaks were integrated using Sciex OS 3.3.0 software (Sciex). Peaks were only selected when their intensity exceeded a 5:1 signal to noise ratio with at least 7 data points across the peak. The ratio of analyte peak areas to internal standard was taken and lipids quantified using a standard curve made up and run at the same time as the samples. Each oxylin was then standardized with weight of the small intestine tissue. Absolute eicosanoid levels from individual intestine samples that were detected by LC-MS/MS in two independent experiments were presented as indicated in Figure S3B, and summarized eicosanoid levels in each treatment groups were presented in Figure 1K. Absolute eicosanoid levels were also scaled to the young control group in respective independent experiment and relative eicosanoid levels in each treatment group are also presented in Figure 1L.

Bulk RNA-seq

RNA was extracted from mouse ileal tissues using the Qiagen Mini RNA kit (Qiagen) according to the manufacturer's instructions. mRNA library preparation (poly A enrichment) and sequencing was performed on the NovaSeq 6000 system (150PE) by Novogene. After a quality control by FastQC, Trim Galore were used to trim raw sequencing data (https://www.bioinformatics.babraham.ac.uk/projects/trim_galore/). STAR was used to align sequence reads to genome (GRCh38, Ensembl release 103). Gene counts were generated using FeatureCounts. The gene expression table was then processed in R (4.0.3). Symbol and Entrez gene IDs annotation were applied by biomaRt. Differentially expressed genes (DEGs) were calculated by DESeq2 and defined by adjusted P-value < 0.05 and log₂ fold change of > |1|. The functions of DEGs were analysed by clusterProfiler within Kyoto Encyclopedia of Genes and Genomes (KEGG) database and Molecular Signatures Database (MSigDB) hallmark gene set. Genetic markers for different signaling pathways or cell subtypes were collected from previous reports and publications. Gene counts were transformed to transcript

per million (TPM) at a logarithmic scale. Deconvolution algorithm single-sample GSEA (ssGSEA) was used to estimate proportions of different cell subtypes across samples.⁶⁹ Wilcoxon-test was used to compare the differences.

Single-cell RNA-seq and data analysis

Young and middle-aged B6 Albino mice were injected i.p. with α CD3 or vehicle control, and single live CD45⁺Ly6G⁻ immune cells were sorted from small intestinal lamina propria by flow cytometry 3 days later. 15,000 cells containing index oligonucleotides were used to prepare single-cell RNA libraries using the Chromium Single Cell 3' Library Kit v3.1 with feature barcode technology for cell multiplexing. Sequencing was performed on the NextSeq 2000 platform (Illumina Inc, #SY-415-1002) using the NextSeq 1000/2000 P³ Reagents (100 cycles) v3 Kit (#20040559). GEX libraries and CMO libraries were each pooled in equimolar quantities and then GEX and CMO pools were further pooled at a ratio of 7:1 (GEX:CMO). PhiX Control v3 (#FC-110-3001) was spiked into the run at a concentration of ~1% to help with cluster resolution and facilitate troubleshooting in case of any problems with the run. Base call data generated by the NextSeq 1000/2000 Control Software (Version 1.5.0.42699) was used to generate FASTQ files using cellranger mkfastq (version 7.1.0). Read alignment and demultiplexing were performed with "cellranger -multi" using the reference genome refdata-gex-GRCm39-2024-A, provided by 10X Genomics. High-quality cells characterized by FDR <0.01 for each cell barcode, >250 unique molecular identifier (UMI) features, <5.02% of mitochondrial genes, number of genes versus UMIs being linear fitted, and doublets being filtered out were selected for further analysis. Count matrix data were normalised by the LogNormalisation function and integrated by the harmony method based on the 2000 highly variable genes. Principal component analysis (PCA) was used to reduce dimensionality and cells were clustered using the Louvain clustering algorithm with resolution of 0.8. UMAP, heatmap and dot plot visualizations were generated on the Trailmaker™ platform (Parse Biosciences, available at <http://app.trailmaker.parsebiosciences.com>, February 2025).

16S rRNA and shotgun metagenomic sequencing

Microbial genomic DNA was extracted from gut contents using DNeasy PowerLyzer PowerSoil Kit (Qiagen). Amplicon sequencing was performed by the Integrated Microbiome Resource (IMR) using the MiSeq system. The 16S rRNA sequencing data was processed with QIIME2. Raw paired-end reads were trimmed and denoised using cutadapt and DADA2.⁷⁰ A naive Bayes classifier trained on the Silva v138 database (<https://www.arb-silva.de/documentation/release-138/>) was used to assign taxonomy to features. Scikit-learn was used to verify the classifier, and the operational taxonomic unit (OTU) table was output. Phyloseq was used to estimate the diversity within and between samples.⁷¹ The Alpha diversity was quantified by Shannon indices for comparison by Mann Whitney test. The beta diversity was estimated by the Bray-Curtis distance and tested by permutational multivariate analysis of variance. The frequencies of each fragment were normalized by the DESeq2 algorithm.

Metagenomic sequencing was performed by the Novogene (UK) Company using the Illumina Novaseq system. Short-read sequencing was conducted on all samples using a NovaSeq producing paired-end 150 bp reads. Quality of sequences was evaluated using FastQC (v.0.11.8, <https://www.bioinformatics.babraham.ac.uk/projects/fastqc/2010>) and MultiQC (v.1.6).⁷² Quality control was performed using fastp (options: -detect_adapter_for_pe -l 30 -q 20 -g -poly_g_min_len 10) (v. 0.24.0).⁷³ Host reads were removed using BWA (v. 0.7.18)⁷⁴ and samtools (options: fastq -f 12) (v.1.21),⁷⁵ mapping against the *Mus musculus* genome (GRCm39). Metaphlan4⁷⁶ was used to assign taxonomy to reads (v.4.1.1, database downloaded on 14th November 2024, options: -subsampling 89000 -subsampling_seed 75646). Beta (Bray-Curtis dissimilarity) and alpha (Shannon and Simpson) diversity metrics were calculated on the species level assignments using the vegan package⁷⁷ in R. PERMANOVA analyses (adonis2) were used to test differences in beta-diversity between groups, and the Kruskal-Wallis rank sum test was used to test differences in alpha diversity. The command cmdscale was used to calculate PCOA coordinates, based on Bray-Curtis values.

Gene expression analysis of human intestinal biopsies

Expression of PGE₂-related genes (synthases, degrading enzymes, and receptors) were analyzed on ileal and colonic mucosal biopsies from patients with active Crohn's disease (CD) and healthy controls,²⁸ using raw microarray data from Gene Expression Omnibus (GEO) dataset GSE16879. ANOVA followed by Holm-Sidak's post-hoc test was used to compare gene expression levels between healthy controls and CD patients pre-treatment, classified as either responsive or refractory to anti-TNF therapy. Additionally, for patients receiving anti-TNF therapy, pre- and post-treatment gene expressions were compared using a paired two-sided Student's t-test. Expression of PGE₂-related genes was also examined in a study by Noble et al., which utilized intestinal biopsies from patients with CD and control subjects without IBD.⁷⁸ Raw microarray data were retrieved from GEO dataset GSE20881. A PGE₂ signature score was calculated using genes that included *PTGS1*, *PTGS2*, *PTGES*, *PTGER2*, and *PTGER4*. Expression of PGE₂-related genes in specific immune cells was assessed in studies by Martin et al.⁷⁸ and Thomas et al.,²⁹ on intestinal biopsies from patients with CD and colitis induced by immune checkpoint blockade (ICB), respectively. The raw single-cell RNA sequencing (scRNA-seq) data were sourced from the Gene Expression Omnibus datasets GSE134809 and GSE206301. Expression of *PTGS2* and immune cell signatures were analyzed in a study by Zhou et al.,³⁰ which utilized intestinal biopsies from patients with and without ICB-induced colitis, using NanoString technology. Correlations between *PTGS2* expression and various immune cell subset signatures were determined using two-tailed Spearman correlation analysis. The gene markers for pathogenic T cell signatures included *IFNG*, *TNF*, *CSF2*, *IL17F*, *STAT4*, *TBX21*, *STAT1*, *IL12RB1*, *IL12RB2*, *IL23R*, and *CXCR3*; homeostatic T cell signature markers were

IL17A, *RORC*, and *MAF*; inflammatory MNP signature markers included *CD14*, *CD80*, *CD86*, *IL1A*, *IL1B*, *IL1R1*, *IL1RN*, *IL6*, *IL12A*, *IL12B*, *IL23A*, *FCGR1A*, and *TREM1*; and anti-inflammatory MNP signature markers were *PPARG*, *MERTK*, *MRC1*, *FCER2*, *IL4R*, *IL13RA1*, *TRAF6*, and *STAT6*.

Gene expression and real-time qPCR

RNA purification from sorted MNPs was performed using the RNeasy Mini Kit (QIAGEN). Complementary DNA (cDNA) was obtained by reverse transcription using the High-Capacity cDNA Reverse Transcription Kits (ThermoFisher Scientific). Microbial gDNA samples were analyzed by real-time PCR using GoTaq qPCR Master Mix (Promega) on the Applied Biosystem 7900HT Fast machine or ThermoFisher QuantStudio 5 real-time PCR system. *Tnf* mRNA expression was normalized to *Gapdh*, while microbial abundance was normalized to universal 16S total bacteria. All qPCR data were presented as relative expression to the control group by the $2^{-\Delta\Delta C_t}$ method. Primers used are enclosed in [Table S1](#).

Scanning electron microscopy

Mouse ilea were fixed in a solution of 3% glutaraldehyde in 0.1 M sodium cacodylate buffer (pH 7.3) for 2 hours. After wash 3 times in 0.1 M sodium cacodylate buffer for 10 min, samples were then postfixated in 1% osmium tetroxide in 0.1 M sodium cacodylate buffer for 45 minutes. A further 3 times washes were performed in 0.1 M sodium cacodylate buffer for 10 min. Dehydration in graded concentrations of acetone (50%, 70%, 90%, and 3 x 100%) for 10 minutes each was followed by critical point drying using liquid carbon dioxide. After mounting on aluminium stubs with carbon tabs attached, the specimens were sputter coated with 20 nm gold palladium and viewed using a Zeiss Crossbeam 550 focused ion beam scanning electron microscope.

QUANTIFICATION AND STATISTICAL ANALYSIS

Fold changes of ratios, including mRNA expression and microbial abundance except relative eicosanoid amounts, were transformed logarithmically prior to statistical analysis. Data were expressed as mean \pm SEM or indicated in the figure legends. Statistical significance between two groups was examined by the unpaired two-tailed Student's *t*-test or Mann-Whitney test and between multiple groups by one-way and two-way analysis of variance (ANOVA) with Holm-Sidak's multiple comparisons tests, while extra sum-of-squares F test was used to evaluate body weight changes among different treatment groups. Statistical work was performed using GraphPad Prism (version 9 or 10) and a *p* value of less than 0.05 was considered as significant.